Estimates of ikaite export from sea ice to the underlying seawater in a sea ice-seawater mesocosm

Geilfus N.-X.[1,2], Galley R. J.[1], Else B. G. T.[3], Campbell K.[1], Papakyriakou T.[1], Crabeck O.[1], Lemes M.[1], Delille B.[4], Rysgaard S.[1,2,5]

[1] Centre for Earth Observation Science, Department of Environment and Geography, University of Manitoba, Winnipeg, Canada
[2] Arctic Research Centre, Aarhus University, Aarhus, Denmark
[3] Department of Geography, University of Calgary, Calgary, Canada
[4] Unité d'Océanographie Chimique, Université de Liège, Liège, Belgium
[5] Greenland Climate Research Centre, Greenland Institute of Natural Resources, Nuuk, Greenland

1. Abstract

The precipitation of ikaite and its fate within sea ice is still poorly understood. We quantify temporal inorganic carbon dynamics in sea ice from initial formation to its melt in a sea ice-seawater mesocosm pool from 11 to 29 January 2013. Based on measurements of total alkalinity (TA) and total dissolved inorganic carbon (TCO_2), the main processes affecting inorganic carbon dynamics within sea ice were ikaite precipitation and CO_2 exchange with the atmosphere. In the underlying seawater, the dissolution of ikaite was the main process affecting inorganic carbon dynamics. Sea ice acted as an active layer, releasing CO_2 to the atmosphere during the growth phase, taking up CO_2 as it melted and exporting both ikaite and TCO_2 into the underlying seawater during the whole experiment. Ikaite precipitation of up to 167 µmol kg^{-1} within sea ice was estimated while its export and dissolution into the underlying seawater was responsible for a TA increase of 64 to 66 µmol kg^{-1} in the water column. The export of TCO_2 from sea ice to the water column increased the underlying seawater TCO_2 by 43.5 µmol kg^{-1}, suggesting that almost all of the TCO_2 that left the sea ice was exported to the underlying seawater. The export of ikaite from the ice to the underlying seawater was associated with brine rejection during sea ice growth, increased vertical connectivity in sea ice due to the upward percolation of seawater, and meltwater flushing during sea ice melt. Based on the change in TA in the water column around the onset of sea ice melt, more than half of the total ikaite precipitated in the ice during sea ice growth was still contained in the ice when the sea ice began to melt. Ikaite crystal dissolution in the water column kept the seawater pCO_2 undersaturated with respect to the atmosphere in spite of increased salinity, TA, and TCO_2 associated with sea ice growth. Results indicate that ikaite export from sea ice and its dissolution in the

underlying seawater can potentially hamper the effect of oceanic acidification on the aragonite saturation state ($\Omega_{aragonite}$) in fall and winter in ice-covered areas, at the time when $\Omega_{aragonite}$ is smallest.

2. Introduction

Currently, each year, 7 Pg of anthropogenic carbon are released to the atmosphere, 29% of which is estimated to be taken up by the Oceans through physical, chemical and biological processes (Sabine et al., 2004). The Arctic Ocean are taking up -66 to -199 Tg C $year^{-1}$, (where a negative value indicates an uptake of atmospheric CO_2) contributing 5-14% to the global ocean CO_2 uptake (Bates and Mathis, 2009), primarily through primary production and surface cooling (MacGilchrist et al., 2014). However, polar ocean CO_2 uptake estimates consider sea ice as an impermeable barrier, ignoring the potential role of ice-covered areas on gas exchange between the ocean and atmosphere. Recent studies have shown that sea ice covered areas participate in the variable sequestration of atmospheric CO_2 into the mixed layer below the ice (e.g. Papakyriakou and Miller 2011; Geilfus et al., 2012; Nomura et al., 2013; Delille et al., 2014; Geilfus et al., 2014; 2015). Studies are required to elucidate the processes responsible as well as their magnitudes both temporally and spatially.

The carbonate chemistry in sea ice and brine is spatially and temporally variable, which leads to complex CO_2 dynamics with the potential to affect the air-sea CO_2 flux (Parmentier et al., 2013). Release of CO_2 from sea ice to the atmosphere has been reported during sea ice formation from open water (Geilfus et al., 2013a) and in winter (Miller et al., 2011; Fransson et al., 2013) while uptake of CO_2 by sea ice from the atmosphere has been reported after sea ice melt onset (e.g. Semiletov et al., 2004; Nomura et al., 2010; Geilfus et al., 2012; Nomura et al., 2013; Fransson et al., 2013; Geilfus et al., 2014; 2015). In combination, these works suggest that the temporal cycle of sea ice formation and melt affects atmospheric CO_2 uptake by the ocean in variable ways. Sea ice may also act as an important control on the partial pressure of CO_2 (pCO_2) in the sea surface through a sea ice pump (Rysgaard et al., 2007). During the earliest stages of sea ice formation, a small fraction of CO_2-supersaturated brine is expelled upward onto the ice surface promoting a release of CO_2 to the atmosphere (Geilfus et al., 2013a). As sea ice forms and grows thicker, salts are partly rejected from the sea ice to the underlying seawater and partly trapped within the sea ice structure, concentrated in brine pockets, tubes and channels. As a result, the concentration of dissolved salts, including inorganic carbon, increase within the brine and promote the precipitation of calcium carbonate crystals such as ikaite ($CaCO_3 \bullet 6H_2O$) (Marion 2001). These crystals have been reported in both natural (Dieckmann et al., 2008; Nomura et al., 2013, Søgaard et al., 2013)

and experimental sea ice (Geilfus et al., 2013b; Rysgaard et al., 2014) and have been suggested to be a key component of the carbonate system (Rysgaard et al., 2007; Fransson et al., 2013; Delille et al., 2014).

During ikaite precipitation within sea ice, TA in brine is reduced by 2 moles due to the reduction of bicarbonate (HCO_3^-) while TCO_2 in brine is only reduced by 1 mole (equation 1 to 3).

$$Ca^{2+} + 2HCO_3^- + 5H_2O \rightleftharpoons CaCO_3 \cdot 6H_2O + CO_2 \quad (1)$$

$$TCO_2 = [HCO_3^-] + [CO_3^{2-}] + [CO_2] \quad (2)$$

$$TA = [HCO_3^-] + 2[CO_3^{2-}] + [B(OH)_4^-] + [OH^-] - [H^+] \quad (3)$$

The specific conditions leading to ikaite precipitation as well as the fate of these precipitates in sea ice are still not fully understood. Ikaite crystals may remain within the ice structure while the CO_2 formed during their precipitation is likely rejected with dense brine to the underlying seawater and sequestered below the mixed layer. During sea ice melt, the dissolution of these crystals triggered by increased ice temperatures and decreased bulk ice salinity will consume CO_2 and drive a CO_2 uptake from the atmosphere to the ice. Such mechanism could be an effective sea ice pump of atmospheric CO_2 (Delille et al., 2014). In addition, ikaite stored in the ice matrix could become a source of TA to the near-surface ocean upon its subsequent dissolution during sea ice melt (Rysgaard et al., 2007; 2009).

The main air-sea fluxes of CO_2 and TCO_2 are driven by brine rejection to the underlying seawater and its contribution to intermediate and deep-water formation (Semiletov et al., 2004; Rysgaard et al., 2007, 2009; Fransson et al., 2013) or below sea ice in ice tank studies (e.g. Killawee et al., 1998 and Papadimitriou et al., 2004). As sea ice thickens, reduced near-surface ice temperatures result in reduced brine volume content, increased brine salinity and increased solute concentration in the brine. In the spring-summer, as the ice temperature increases, sea ice brine volume increases and sea ice becomes vertically permeable to liquid (Golden et al., 2007), enhancing the potential CO_2 exchange between the atmosphere, sea ice and ocean. Eventually internal ice melt promotes brine dilution, which decreases brine salinity, TA, TCO_2, and leads to lower pCO_2 in the brine. In addition, the dissolution of ikaite decreases brine pCO_2 (Eq. 1) (Geilfus et al., 2012; 2015). These conditions all favour sea ice as a sink for atmospheric CO_2 (Nomura et al., 2010; Geilfus et al., 2012; Nomura et al., 2013; Geilfus et al., 2015). Melting sea ice stratifies surface seawater leading to decreased TA, TCO_2 and pCO_2, in the sea surface, enhancing air-sea CO_2 fluxes (Rysgaard et al., 2007; 2009).

89 Although we now have a basic understanding of the key mechanisms of carbon cycling in sea ice,
90 significant unknowns remain. One of the major unknowns is the fate of ikaite, TCO_2 and CO_2 released
91 from sea ice during winter. It is unclear what proportion of precipitated ikaite crystals in sea ice remain in
92 the matrix to be released upon melt or what proportion are expelled with brine drainage during ice
93 formation and growth. Examining the chemical signatures of the water column beneath sea ice may
94 provide an indication of the importance of the different processes. However, the signal of carbon
95 components released from 1-2 meters of sea ice growth is difficult to detect in a water column several
96 hundred meters deep.

97 In this study, we followed the evolution of the inorganic carbon dynamics within experimental sea ice
98 from sea ice formation to melt in a sea ice-seawater mesocosm pool (~435 m^3). The benefits of this type
99 of environment are multiple. An artificial pool equipped with a movable bridge makes it possible to
100 collect undisturbed samples from thin growing sea ice. We gain the ability to carefully track carbonate
101 parameters in the ice, in the atmosphere, and in the underlying seawater, while growing sea ice in a large
102 volume of seawater, so that conditions closely mimic the natural system. During this experiment, we
103 examined physical and chemical processes, in the absence of biology, responsible for changes in the
104 inorganic carbon system of sea ice and the underlying seawater and quantify fluxes of inorganic carbon
105 between the atmosphere, sea ice and the water column. We also discuss that dissolution of ikaite crystals
106 exported from sea ice in the underlying seawater can potentially hamper the effect of oceanic
107 acidification on $\Omega_{aragonite}$.

108 **3. Site description, sampling and analysis**

109 The Sea-ice Environmental Research Facility (SERF) is an in-ground outdoor concrete pool of 18.3 m
110 by 9.1 m in surface area and 2.6 m deep exposed to ambient temperatures, winds and solar radiation (by
111 retracting its roof, Fig. 1). The weather conditions in the region are conducive to sea ice growth for
112 several months every winter. Prior to the experiment, the pool is filled with artificial seawater (ASW)
113 made by dissolving large quantities of various rock salts into local groundwater to mimic the major
114 composition of natural seawater (see Rysgaard et al., (2014) for exact composition of the ASW). Sea ice
115 is melted in the pool by circulating heated ethylene glycol through a closed-loop hose located at the
116 bottom of the pool, allowing successive ice growth/melt experiments to be carried out during one winter.
117 The experimental sea ice and brine exhibit similar physical and chemical properties to those observed in
118 natural Arctic sea ice (Geilfus et al., 2013; Hare et al., 2013). The experiment described herein was

initiated from open water conditions on 11 January 2013 when the heater was turned off. Sea ice grew until 26 January when the heat was turned back on. The experiment ended on 30 January when the pool was 20% ice-free.

Four 375 W pumps were installed on the bottom of the pool near each of the corners to induce a consistent current. The pumps were configured to draw water from their base and then propel it outward parallel to the bottom of the pool. The pumps were oriented successively at right angles to one another, which created a counterclockwise circulation of 2-3 cm s^{-1} (Else et al., 2015).

Bulk ice and seawater temperatures were recorded by an automated type-T thermocouple array fixed vertically in the pool. Seawater salinity was measured continuously using Aanderaa CT sensors (model 4319) located at 30, 100, 175 and 245 cm depth. The in situ seawater pCO_2 was measured every 5 sec using a Contros HydroC (resolution < 1 µatm, accuracy ± 1% of the upper range value) located at 1.3 m depth.

Air temperature and relative humidity were measured using a Vaisala HMP45C probe at a meteorological station located 2 m above the sea ice surface. Solar irradiance was continuously recorded by an Eppley Precision Spectral Pyranometer (range=0.285–2.8 µm) mounted 10 m above the sea ice surface. In addition, estimated photosynthetically active radiation (PAR) values at the ice bottom were recorded with Alec mkv-L PAR sensors throughout the study and ranged from 0 to 892 µmol photons m^{-2} s^{-1}.

Sea ice and seawater samples were obtained from a confined area located on the North side of the pool to minimize effects on other experiments (e.g. Else et al., 2015). Ice samples were collected using ceramic knives or a Kovacs Mark II coring system depending on the ice thickness. Sampling was performed from a movable bridge to avoid walking on the ice surface and to ensure only undisturbed sites were sampled. Ice cores were collected from one end of the pool (half meter away from the edge of the pool) and at least 20 cm away from previous cored sites. Ice cores were packed in clean plastic bags and kept frozen during the 20 minutes transport to a cold laboratory and processed within a few hours. Seawater was sampled for total alkalinity (TA) and total dissolved inorganic carbon (TCO_2) with a peristaltic pump (Cole Palmer, Masterflex-Environment sampler, equipped with PTFE tubing) through an ice core hole the ice-water interface, at 1.25 m, and 2.5 m depth. Samples were stored in 12 ml gas-tight

147 vials (Exetainer, Labco High Wycombe, UK) and poisoned with 12 µl of saturated $HgCl_2$ solution and
148 stored in the dark at 4°C until analysed.

149 Air-ice CO_2 fluxes were measured using a Li-Cor 8100-103 chamber associated with a LI-8100A soil
150 CO_2 flux systems. The chamber was connected in a closed loop to the IRGA with an air pump rate of 3 L
151 min^{-1}. The measurement of pCO_2 in the chamber was recorded every sec over a 15 minute period. The
152 flux was computed from the slope of the linear regression of pCO_2 against time (r^2>0.99) according to
153 Frankignoulle (1988), taking into account the volume of ice or snow enclosed within the chamber. The
154 uncertainty of the flux computation due to the standard error on the regression slope was on average ±3%.

155 In the cold laboratory, sea ice cores were cut into 2 cm sections using a pre-cleaned stainless steel
156 band saw. Each section was placed in a gas-tight laminated (Nylon, ethylene vinyl alcohol and
157 polyethylene) plastic bag (Hansen et al., 2000) fitted with a gastight Tygon tube and a valve for sampling.
158 The plastic bag was sealed immediately and excess air was gently removed through the valve using a
159 vacuum pump. The bagged sea ice samples were then melted in the dark at 4°C to minimize the
160 dissolution of calcium carbonate precipitates (meltwater temperature never rose significantly above 0°C).
161 Once melted, the meltwater mixture and bubbles were transferred to gas-tight vials (12 ml Exetainer,
162 Labco High Wycombe, UK), poisoned with 12 µl solution of saturated $HgCl_2$ and stored in the dark at
163 4°C until analysed.

164 Bulk ice and seawater salinities were measured using a Thermo Orion 3-star with an Orion
165 013610MD conductivity cell and values were converted to bulk salinity (Grasshoff et al., 1983). TA was
166 determined by potentiometric titration (Haraldsson et al., 1997) while TCO_2 was measured on a
167 coulometer (Johnson et al., 1987). Routine analysis of Certified Reference Materials provided by A. G.
168 Dickson, Scripps Institution of Oceanography, verified that TA and TCO_2 were analyzed within ±3 and
169 ±2 µmol kg^{-1}, respectively. Brine volume was estimated from measurements of bulk salinity, temperature
170 and density according to Cox and Weeks (1983) for temperatures below -2°C and according to
171 Leppäranta and Manninen (1988) for ice temperatures within the range -2 to 0°C.

172 Bulk ice samples for biological measurements were collected between 14 and 21 January. Filtered
173 (0.2 µm) SERF seawater (FSW) was added at a ratio of 3 parts FSW to 1 part ice and the samples were
174 left to melt in the dark. Chlorophyll *a* was determined on three occasions by filtering two aliquots of the
175 melted ice sample onto GF/F filters (Whatmann brand) and extracting pigments in 10 ml of 90% acetone

for 24 h. Fluorescence was measured before and after the addition of 5% HCl (Turner Designs Fluorometer) and Chl *a* concentration was calculated following Parsons et al. (1984). Measurements of bacterial production were done four times during the biological sampling period by incubating 6-10 ml subsamples of the ice-FSW solution with ^{3}H-leucine (final concentration of 10 nM) for 3h at 0°C in darkness (Kirchmann, 2001). Half of the samples were spiked with trichloroacetic acid (TCA, final concentration 5%) as controls prior to the incubation, while the remaining active subsamples were fixed with TCA (final concentration 5%) after incubation. Following the incubation, vials were placed in 80°C water for 15 minutes (Garneau et al., 2006) before filtration through 0.2 μm cellulose acetate membranes (Whatmann brand) and rinsing with 5% TCA and 95% ethanol. Filters were dried and dissolved in scintillation vials by adding 1 ml ethyl acetate, and radioactivity was measured on a liquid scintillation counter after an extraction period of 24 h. Bacterial production was calculated using the equations of Kirchman (1993) and a conversion factor of 1.5 kg C mol^{-1} (Ducklow et al., 2003).

4. Results

4.1. Sea ice and seawater physical conditions

Sea ice was grown in the pool from open water on 13 January 2013 and reached a maximum thickness of 24 cm on 26 January at which point the heat at the base of the pool was turned on. On 30 January the experiment ended with the pool 20% ice-free. Three main snowfall events occurred during the experiment. The first, from 14 to 15 January, covered the sea ice surface with 1 cm of snow. The second, from 18 to 23 January, deposited 6-9 cm of snow over the entire pool. On the morning of 23 January, the snow was manually cleared off the ice surface to investigate the insulating effect of the snow on the ice temperature and ikaite precipitation (Rysgaard et al., 2014). Finally, from noon on 24 January to 27 January, 8 cm of snow covered the entire pool until the end of the experiment on 30 January.

The air temperature at the beginning of the experiment ranged from -2°C to -26°C, which initiated rapid sea ice growth to 15 cm until 18 January (Fig. 2). During this initial sea ice growth, the sea ice was attached to the side of the pool resulting in the development of a hydrostatic pressure head that caused percolation of seawater at the freezing point upwards through the sea ice volume as the sea ice grew downwards. This resulted in repeated events of increased sea ice temperature from the bottom to the surface observed between 15 and 18 January (Fig. 2). Subsequently, the ice was cut using an ice saw around the perimeter, allowing the ice to float and a pressure release valve was installed to prevent such

events (Rysgaard et al., 2014). During this period, the ice temperature oscillated between relatively warm (~ -3°C) and cold (~ -7°C) phases. Brine volume content (0.047) was low in the middle part of the ice cover, close to the permeability threshold of 0.05 as suggested by Golden et al., (2007). The bulk ice salinity profiles were typically C-shaped with values ranging from 6 to 23 (Fig. 2). The underlying seawater salinity increased rapidly due to sea ice growth. From 18 to 23 January, the 9 cm snow cover insulated the ice cover from the cold atmosphere (Rysgaard et al., 2014), resulting in a fairly constant ice thickness, nearly no change in ice temperature and salinity, a brine volume content above the permeability threshold and a small increase in the underlying seawater salinity. Once the ice surface was cleared of snow on the morning of 23 January, the ice temperature decreased throughout the entire ice thickness and the ice surface salinity increased. The sea ice volume cooled from the top downwards, and the brine volume content decreased below the permeability threshold on 23 January and rapid sea ice growth rapidly increased the seawater salinity. Shortly after the snow clearing, the last snowfall event covered the ice surface with 8 cm of snow, reducing the effect of the cold atmosphere on the ice cover. On 26 January, the heater was activated to initiate sea ice melt. Sea ice temperatures increased and became isothermal around -2°C while the bulk ice salinity decreased and the brine volume content increased up to 0.13. The sea ice melt decreased the seawater salinity. The pool was well mixed during the whole growth phase with similar salinity and temperature observed at the four depths. However, once the heat was turned on, the pool become stratified with respect to salinity changes, as the salinity at 30 cm depth started to diverge from the deeper depths (Fig. 2).

4.2. Carbonate system

TA and TCO_2 in seawater, noted as $TA_{(sw)}$ and $TCO_{2(sw)}$, were sampled at the sea ice-seawater interface, 1.25 and 2.5 m depth. An ANOVA test over the 3 depths revealed that the means are not statistically different ($p<0.01$) so we consider the average concentration of the three depths in the following analysis. During sea ice growth, $TA_{(sw)}$ increased from 2449 to 2644 µmol kg^{-1} (black line, Fig. 3a) while $TCO_{2(sw)}$ increased from 2347 to 2516 µmol kg^{-1} (black line, Fig. 3b). Once the ice started to melt, $TA_{(sw)}$ decreased to 2607 µmol kg^{-1} and $TCO_{2(sw)}$ decreased to 2461 µmol kg^{-1}. As the experiment stopped before the ice was completely melted in the tank, both the seawater salinity and $TA_{(sw)}$ do not reach their initial values at the end of the experiment (Table 1, Fig 2 and 3). To discard the effect of salinity changes, we normalized $TA_{(sw)}$ and $TCO_{2(sw)}$ to a salinity of 33 (noted as $nTA_{(sw)}$ and $nTCO_{2(sw)}$) according to the equations 4 and 5:

$$n\mathrm{TA}_{(sample)\,t} = \frac{\mathrm{TA}_{(sample)\,t}}{\mathrm{S}_{(sample)\,t}} \times 33 \quad (4)$$

$$n\mathit{T}\mathrm{CO}_{2\,(sample)\,t} = \frac{\mathit{T}\mathrm{CO}_{2\,(sample)\,t}}{\mathrm{S}_{(sample)\,t}} \times 33 \quad (5)$$

where t is the time of the sampling and S the salinity of the sample (seawater or sea ice). During ice growth, $n\mathrm{TA}_{(sw)}$ and $n\mathit{T}\mathrm{CO}_{2(sw)}$ increased slightly to 2446 and 2328 µmol kg^{-1}, respectively (Fig. 3c). However, once the ice started to melt, $n\mathrm{TA}_{(sw)}$ increased to 2546 µmol kg^{-1} and $n\mathit{T}\mathrm{CO}_{2(sw)}$ increased to 2404 µmol kg^{-1}.

The in situ $p\mathrm{CO}_2$ of the underlying seawater ($p\mathrm{CO}_{2(sw)}$) decreased from 377 to 360 µatm as the seawater temperature in the pool decreased to the freezing point. The $p\mathrm{CO}_{2(sw)}$ then oscillated from 360 to 365 µatm during sea ice growth. One day after the heater was turned on, the $p\mathrm{CO}_{2(sw)}$ increased to a similar concentration as at the beginning of the experiment before decreasing to 373 µatm by the end of the experiment (Fig. 3d).

Within bulk sea ice, $\mathrm{TA}_{(ice)}$ ranged from 300 to 1907 µmol kg^{-1} while $\mathit{T}\mathrm{CO}_{2(ice)}$ ranged from 237 to 1685 µmol kg^{-1}. Both $\mathrm{TA}_{(ice)}$ and $\mathit{T}\mathrm{CO}_{2(ice)}$ exhibited C-shaped profiles with higher concentrations at the surface and bottom layers of the ice cover (Fig. 4). The concentration of $\mathrm{TA}_{(ice)}$ (average = 476 µmol kg^{-1}) and $\mathit{T}\mathrm{CO}_{2(ice)}$ (average = 408 µmol kg^{-1}) did not show significant variability during our survey, except at the surface of the ice. A first maximum was observed on 17 January with concentration of 1907 µmol kg^{-1} for TA and 1685 µmol kg^{-1} for $\mathit{T}\mathrm{CO}_2$. A second maximum was observed on 23 January with concentration of 1433 µmol kg^{-1} for TA and 861 µmol kg^{-1} for $\mathit{T}\mathrm{CO}_2$. These maxima matched the high bulk ice salinity (Fig. 2), so we also normalized $\mathrm{TA}_{(ice)}$ and $\mathit{T}\mathrm{CO}_{2(ice)}$ (noted as $n\mathrm{TA}_{(ice)}$ and $n\mathit{T}\mathrm{CO}_{2(ice)}$, Fig. 4) to a salinity of 33 (according to the equations 4 and 5) to discard the effect of salinity changes and facilitate comparison with the underlying seawater. During initial sea ice formation (up to 17 January), the concentration of both $n\mathrm{TA}_{(ice)}$ (from 1083 to 2741, average = 1939 µmol kg^{-1}) and $n\mathit{T}\mathrm{CO}_{2(ice)}$ (from 853 to 2440, average = 1596 µmol kg^{-1}) were at their minima in the experimental time series. From 17 to 21 January, both $n\mathrm{TA}_{(ice)}$ and $n\mathit{T}\mathrm{CO}_{2(ice)}$ increased throughout the ice column (average $n\mathrm{TA}_{(ice)}$ = 2375 µmol kg^{-1} and $n\mathit{T}\mathrm{CO}_{2(ice)}$ = 2117 µmol kg^{-1}). However, from 21 January until the initial sea ice melt, $n\mathrm{TA}_{(ice)}$ and $n\mathit{T}\mathrm{CO}_{2(ice)}$ decreased in the top 5 cm of the ice cover (average $n\mathrm{TA}_{(ice)}$ = 2125 µmol kg^{-1} and $n\mathit{T}\mathrm{CO}_{2(ice)}$ = 1635 µmol kg^{-1}).

4.3. Air-ice CO_2 fluxes

263 The CO_2 fluxes measured at the variably snow-covered sea ice surface (Fig. 2b), ranged from 0.29 to
264 4.43 mmol m^{-2} d^{-1} show that growing sea ice released CO_2 to the atmosphere (Fig. 5). However, as soon
265 as the ice started to warm up and then melt, the sea ice switched from source to sink for atmospheric CO_2
266 with downward fluxes from -1.3 to -2.8 mmol m^{-2} d^{-1}. These ranges of air-ice CO_2 exchanges are of the
267 same order of magnitude as fluxes reported on natural sea ice using the same chamber technique in the
268 Arctic during the initial sea ice growth (from 4.2 to 9.9 mmol m^{-2} d^{-1} in Geilfus et al., 2013) and during
269 the spring-summer transition (from -1.4 to -5.4 mmol m^{-2} d^{-1} in Geilfus et al., 2015). In Antarctica air-ice
270 CO_2 fluxes were reported during the spring-summer transition from 1.9 to -5.2 mmol m^{-2} d^{-1} by Delille et
271 al (2014), from 0.3 to -2.9 mmol m^{-2} d^{-1} (Geilfus et al., 2014) and from 0.5 to -4 mmol m^{-2} d^{-1} (Nomura et
272 al., 2013).

273 **5. Discussion**

274 **5.1. Key processes affecting the carbonate system**

275 The dynamics of inorganic carbon in the ocean and sea ice are mainly affected by temperature and
276 salinity changes, precipitation and dissolution of calcium carbonate, and biological activities (Zeebe and
277 Wolf-Gladrow, 2001). During this experiment, neither organic matter nor biota were purposely
278 introduced into the pool; the observed range of bulk ice microbial activity (5.7 x 10^{-9} on 14 January to 7.5
279 x 10^{-7} g C L^{-1} h^{-1} on 21 January) and algal Chl *a* (0.008 on 14 January to 0.002 µg L^{-1}on 21 January) were
280 too low to support any biological activity (Rysgaard et al., 2014). Therefore biological activity is unlikely
281 to have played a role. During the same 2013 time series at SERF, Rysgaard et al. (2014) discussed the
282 precipitation of ikaite within the ice cover in detail, reporting high concentrations of ikaite (> 2000 µmol
283 kg^{-1}) at the surface of the ice in brine skim and frost flowers and ikaite precipitation up to 350 µmol kg^{-1}
284 within bulk sea ice. Within sea ice, ikaite precipitation is associated with low ice temperatures, high bulk
285 salinity and high $TA_{(ice)}$ and $TCO_{2(ice)}$ concentrations (Fig. 2 and 3).

286 The main processes affecting the carbonate system can be described by changes in TA and TCO_2
287 (Zeebe and Wolf-Gladrow, 2001). An exchange of $CO_{2(gas)}$ affects TCO_2 while TA remains constant and
288 the precipitation-dissolution of calcium carbonate affects both TA and TCO_2 in a ratio of 2:1 (see
289 equation 1 to 3, Fig. 6). To calculate the theoretical changes in TA and TCO_2 during the course of the
290 experiment, we used seawater samples from 11 January prior to sea ice formation (t=0, Table 1) as the
291 origin point (blue circle on Fig. 6). Sea ice data are located between the theoretical calcium carbonate
292 precipitation line and the CO_2 release line (Fig. 6a) while seawater data mainly fall on the calcium

carbonate dissolution line (Fig. 6b), suggesting that the carbonate system within sea ice is affected by both the precipitation of ikaite and a release of $CO_{2(gas)}$ while the underlying seawater is mainly affected by the dissolution of calcium carbonate.

5.2. Estimation of the precipitation-dissolution of ikaite

During the experiment, Rysgaard et al., (2014) observed ikaite within sea ice using direct microscopic observations. The precipitation-dissolution of ikaite and gas exchange are the only two processes taking place during the experiment. As illustrated in Fig. 6, an exchange of CO_2 does not affect TA while the precipitation-dissolution of ikaite affects TA and TCO_2 in a ratio 2:1. Therefore, we use TA to estimate how much ikaite is precipitated or dissolved within the ice cover and the underlying seawater.

Assuming no biological effect, ikaite precipitation/dissolution and gas exchange, TA and TCO_2 are considered conservative with salinity. Therefore, we can calculate the expected TA and TCO_2 (noted as $TA_{(ice)}^*$ and $TCO_{2(ice)}^*$ in the ice cover and $TA_{(sw)}^*$, $TCO_{2(sw)}^*$ for the water column) based on the initial seawater conditions ($TA_{(sw)}$, $TCO_{2(sw)}$ and $S_{(sw)}$ at t=0, Table 1) and the sample salinity (bulk sea ice or seawater) measured during the experiment:

$$TA^*_{(sample)\,t} = \frac{TA_{(sw)\,t=0}}{S_{(sw)\,t=0}} \times S_{(sample)\,t} \quad (6)$$

$$TCO^*_{2\,(sample)\,t} = \frac{TCO_{2\,(sw)\,t=0}}{S_{(sw)\,t=0}} \times S_{(sample)\,t} \quad (7)$$

where t is the time of the sampling. Within the ice cover, $TA_{(ice)}$, $TCO_{2(ice)}$, and the bulk ice salinity are averaged throughout the ice column at each sampling day (Fig. 7a, b, black line) while for the underlying seawater, we used the averaged $TA_{(sw)}$, $TCO_{2(sw)}$ and salinity for all the measured depths (Fig. 2a, b, black line). The difference between $TA_{(sample)}^*$ and the observed TA is only due to the precipitation or dissolution of ikaite crystals. In case of ikaite precipitation (*i.e.* $TA_{(sample)}^* > TA_{(sample)}$), half of this positive difference corresponds to the amount of ikaite precipitated within the ice. This ikaite may either remain or may be exported out of the ice. A negative difference (*i.e.* $TA_{(sample)}^* < TA_{(sample)}$), indicates ikaite dissolution.

5.2.1. Sea ice

Greater $TA_{(ice)}^*$ and $TCO_{2(ice)}^*$ compared to the averaged observed $TA_{(ice)}$ and $TCO_{2(ice)}$ (Fig. 7a, b) are expected as ikaite is precipitated and CO_2 released from the ice to the atmosphere (Fig. 5, 6). Half the difference between $TA_{(ice)}^*$ and $TA_{(ice)}$ is a result of ikaite precipitation (Fig. 7c, black diamonds). Highly

variable ikaite precipitation was observed (Fig. 7c). Ikaite precipitation was up to 167 µmol kg^{-1} (e.g. first days of the experiment) and as low as 1 µmol kg^{-1} (e.g. 19 January). A negative difference between $TA_{(ice)}^{*}$ and $TA_{(ice)}$ (*i.e.* ikaite dissolution) occurred on three occasions: 14, 20 and after the 26 January (beginning of the sea ice melt). On these occasions, the ice cover was relatively warm due to warmer atmospheric temperatures (14 January), thicker snow cover insulating the ice cover from the cold atmosphere (20 January) or when heat was turned back on (after 26 January, Fig. 2). Relatively high sea ice temperatures likely promote ikaite dissolution in agreement with Rysgaard et al., (2014) who linked ikaite precipitation/dissolution to ice temperature. The upward percolation of seawater observed from 15 to 18 January might complicate the effect of sea ice temperature on ikaite formation because it was in part responsible for increased ice temperatures (Fig. 2b) and therefore increased the sea ice brine volumes (Fig. 2c). Increased vertical connectivity (permeability) of the network of liquid inclusions throughout the sea ice (Golden et al., 2007; Galley et al., 2015) would have allowed the export of ikaite crystals from the ice cover to the underlying seawater. However, while we calculated a negative difference between $TA_{(ice)}^{*}$ and $TA_{(ice)}$, ikaite crystals were observed by Rysgaard et al., (2014). We compared the direct microscopy observations by averaging the amount of ikaite precipitated throughout the ice thickness for each sampling day from Rysgaard et al., (2014) (Fig. 7c, white dots) with our estimation of the amount of ikaite based on the difference between $TA_{(ice)}^{*}$ and $TA_{(ice)}$ (Fig. 7c, black diamonds). Both ikaite measurements are of the same order of magnitude however the average (22 µmol kg^{-1}) and maximum (100 µmol kg^{-1}) of direct observations presented by Rysgaard et al. (2014) were lower than our estimated average (40 µmol kg^{-1}) and maximum of up to 167 µmol kg^{-1} over this whole experiment. Deviations are likely due to methodological differences. Here, sea ice samples were melted to subsample for TA and TCO_2, Ikaite crystals may have dissolved during melting, leading to an underestimation of the total amount of ikaite precipitated in the ice. However, the difference between $TA_{(ice)}^{*}$ and $TA_{(ice)}$ provides an estimation of how much ikaite is precipitated in the ice cover, including those crystals potentially already exported to the underlying seawater. The method used by Rysgaard et al., (2014) avoid the bias of ikaite dissolution during sea ice melt with the caveat that crystals need to be large enough to be optically detected. If no crystals were observed, Rysgaard et al., (2014) assumed that no crystals were precipitated in the ice, though ikaite crystals could have been formed and then exported into the underlying seawater prior to microscopic observation of the sample, which may explain the difference observed between both methods during initial sea ice formation (15-18 January) when the ice was still very thin. In addition, the

succession of upward percolation events could have facilitated the ikaite export from the ice cover to the underlying seawater. Estimations from both methods show similar concentrations when the ice (i) warmed due to snowfall (18-23 January) and (ii) cooled once the snow was removed (on 23 January). Once the ice started to melt (26 January), Rysgaard et al., (2014) reported a decrease in the ikaite precipitation while in this study we reported a negative difference between $TA_{(ice)}^{*}$ and $TA_{(ice)}$, possibly indicating that ikaite dissolved in the ice.

5.2.2. Water column

The main process affecting the carbonate system in the underlying seawater in this study is the export of ikaite from the ice and its dissolution in the water column (Fig. 6). While a few studies of ikaite precipitation within sea ice carried out over open ocean hypothesized that ikaite remained trapped within the sea ice matrix (Rysgaard et al., 2007; 2013; Delille et al., 2014), the observed increase of $nTA_{(sw)}$ (Fig. 3) suggests that ikaite precipitated within the ice cover was exported to the underlying seawater where the crystals were dissolved as suggested by Fransson et al., (2013). Lower $TA_{(sw)}^{*}$ and $TCO_{2(sw)}^{*}$ compared to $TA_{(sw)}$ and $TCO_{2(sw)}$ (Fig. 3) confirm the dissolution of ikaite in the underlying seawater as the dissolution of ikaite crystals will decrease both TA and TCO_2 (equations 1 to 3). Therefore, half the difference between $TA_{(sw)}^{*}$ and $TA_{(sw)}$ corresponds to the concentration of ikaite exported from the ice and dissolved in the underlying seawater (Fig. 8a). This concentration increased over time to a maximum of 66 µmol kg^{-1}.

During this experiment, $nTA_{(sw)}$ increased by 128 µmol kg^{-1} while $nTCO_{2(sw)}$ increased by 82 µmol kg^{-1} (Fig. 3c). This suggests that 64 µmol kg^{-1} of ikaite are dissolved compared to the 66 µmol kg^{-1} estimated from the difference between $TA_{(sw)}^{*}$ and $TA_{(sw)}$. As a result of the effect of ikaite dissolution on the 2:1 ratio of $TA:TCO_2$, the dissolution of ikaite accounts for the entire increase of $nTA_{(sw)}$ but only accounts for 64-66 µmol kg^{-1} of the 82 µmol kg^{-1} increase in $nTCO_{2(sw)}$. So, 16-18 µmol kg^{-1} (about 25%) of the increase of $nTCO_{2(sw)}$ cannot be explained by the dissolution of ikaite. The increase of both $nTA_{(sw)}$ and $nTCO_{2(sw)}$ is more significant once the ice starts to melt (26 January). During sea ice melt, increased vertical permeability resulting in increased liquid communication through the sea ice volume from below likely in part dissolved ikaite crystals still residing in the ice at that time, and also will have created a downward crystal export mechanism. As the ice melt advanced, patches of open water occurred at the surface of the pool. Therefore, uptake of atmospheric CO_2 by the undersaturated seawater likely occurred, increasing the $TCO_{2(sw)}$.

The dissolution of ikaite crystals could also have a strong impact on the $pCO_{2(sw)}$. The water column was undersaturated compared to the atmosphere during the whole experiment (Fig. 3d). A release of CO_2, from the ice to the atmosphere was measured during sea ice growth (Fig. 5) in spite of the undersaturated $pCO_{2(sw)}$. This suggests that air-ice CO_2 fluxes are only due to the concentration gradient between the ice and the atmosphere (Geilfus et al., 2012; Nomura et al., 2013) but that sea ice exchanges CO_2 with the atmosphere independently of the seawater concentration (Geilfus et al., 2014). The $pCO_{2(sw)}$ is highly correlated with the seawater temperature (Fig. 2) with a rapid decrease of $pCO_{2(sw)}$ during the first days of the experiment (13 to 15 January) and a relative constant $pCO_{2(sw)}$ until 27 January. However, on 26 January, the heat was turned back on affecting the seawater temperature on the same day (Fig. 2) while the impact of increasing temperature on the $pCO_{2(sw)}$ appeared one day later (Fig. 3d). We normalized the $pCO_{2(sw)}$ to a temperature of -1°C (after Copin-Montegut (1988), noted as $npCO_{2(sw)}$, blue line on Fig. 3d). The $npCO_{2(sw)}$, does not show major variations during sea ice growth with values around 380 µatm. However, once the heat is turned on and the seawater temperature increased (on 26 January), $npCO_{2(sw)}$ decreased from 383 µatm to 365 µatm, while $pCO_{2(sw)}$ did not change in response to increased seawater temperatures until 27 January, suggesting that a process other than temperature change affected the $pCO_{2(sw)}$. According to equation 1, the dissolution of calcium carbonate has the potential to reduce $pCO_{2(sw)}$. Therefore, during sea ice growth and the associated release of salt, TA, TCO_2 and ikaite crystals to the underlying seawater, ikaite dissolution within the seawater could be responsible for maintaining stable $pCO_{2(sw)}$ values while seawater salinity, $TA_{(sw)}$ and $TCO_{2(sw)}$ are increasing. Once the seawater temperature increased (26 January), sea ice melt likely released ikaite crystals to the underlying seawater (Fig. 2, 8a) along with brine and meltwater, a process that would continuously export ikaite from the sea ice as the volume interacting with the seawater via percolation or convection increased. The dissolution of these crystals likely contributed to keeping the $pCO_{2(sw)}$ low and counterbalancing the effect of increased temperature. We argued that once all the ikaite crystals are dissolved, the increase seawater temperature increased the $pCO_{2(sw)}$ simultaneously with the $npCO_{2(sw)}$ (27 January, Fig. 3).

5.3. Ikaite export from the ice cover to the water column

We estimated the amount of ikaite precipitated and dissolved within sea ice and seawater based on the sea ice (and seawater) volume (in m^3), the sea ice and seawater density, the concentration of ikaite precipitated and dissolved within the ice cover (Fig. 7c), and the concentration of ikaite dissolved in the water column (Fig. 8a). Within the ice cover, the amount of ikaite precipitated-dissolved ranged from -0.7

411 to 1.97 mol (Fig 8b, Table 2), with a maximum just after the snow was cleared on 23 January. In the
412 underlying seawater, the amount of ikaite dissolved in the pool increased from 0.47 mol on the first day
413 of the experiment to 11.5 mol on 25 January when sea ice growth ceased. Once the ice started to melt the
414 amount of dissolved ikaite increased up to 20.9 (28 Jan) and 26.7 mol (29 January, Table 2). The
415 estimation of ikaite dissolution in the pool is significantly higher than the estimated amount of ikaite
416 precipitated (and potentially exported) within the ice cover, especially during sea ice melt. Within the ice
417 cover, the ikaite values presented here represent a snapshot of the ikaite content in the ice at the time of
418 sampling. In the underlying seawater, ikaite dissolution increased $TA_{(sw)}$ cumulatively over time.

419 The difference between $TA_{(ice)}^{*}$ and $TA_{(ice)}$ provides an estimation of ikaite precipitated within the ice,
420 including potential ikaite export to the underlying seawater, so it cannot be used to determine how much
421 ikaite remained in the ice versus how much dissolved in the water column. However, Rysgaard et al.,
422 (2014) indicate ikaite precipitated within the ice based on direct observations. Using the ikaite
423 concentration reported in Rysgaard et al (2014) (and shown in Fig. 7c), the sea ice volume (in m^3) and
424 density, we calculate that 0 to 3.05 mol of ikaite precipitated within the ice cover during sea ice growth
425 (Fig. 8b and Table 2). This amount decreased to 0.46 and 0.55 mol during the sea ice melt (28 and 29
426 January, respectively). Increased ikaite dissolution in the water column when the ice began to melt (from
427 11.5 to 20.9 mol) indicates that 9.4 mol of ikaite were stored in the ice and rejected upon the sea ice melt.
428 This amount is about three times the amount of ikaite precipitated in the ice estimated by Rysgaard et al.,
429 (2014) at the end of the growth phase (3.05 mol, Table 2), suggesting more work is needed best estimate
430 ikaite precipitation within sea ice.

431 Once the ice started to melt, the increased ikaite dissolution from 11.5 mol to 20.9 mol (28 January) and
432 to 26.7 mol (29 January) suggests that about the same amount of ikaite is dissolved during the sea ice
433 growth as during the first two days of the sea ice melt. The amount of ikaite dissolved in the water
434 column after melt commenced continued to increase cumulatively, suggesting that ikaite is continuously
435 exported to the underlying seawater as increased sea ice temperatures permit more of the volume to
436 communicate with the underlying seawater. Therefore, we can assume that more than half of the amount
437 of ikaite precipitated within the ice remained in the ice cover before ice melt began.

438 **5.4. Air-ice-seawater exchange of inorganic carbon**

SERF is a semi-closed system where the only way for the surface (water or sea ice) to gain or lose CO_2 is through exchange with the atmosphere, making it reasonable to track the exchange of TCO_2 in the atmosphere-sea ice-seawater system. The ice cover always had lower $TCO_{2(ice)}$ during the experiment ($TCO_{2(ice)}^{*} > TCO_{2(ice)}$) compared to what would be expected if the CO_2 simply followed brine rejection in a conservative process (i.e. $TCO_{2(ice)}^{*}$) (Fig. 7b). This could be due to: (i) CO_2 released to the atmosphere from sea ice, (ii) decreased $TCO_{2(ice)}$ due to the precipitation of ikaite within sea ice and/or (iii) sea ice exchanging TCO_2 with the underlying seawater.

The number of moles of TCO_2 exchanged during this experiment was calculated using the sea ice (and seawater) volume (in m^3) and density (in kg/m^3). The total amount of $TCO_{2(ice)}$ lost from the ice cover (the difference between $TCO_{2(ice)}^{*}$ and $TCO_{2(ice)}$) ranged from 0.11 to 6.02 mol (average 2.38 mol, Fig. 9, black dots). The greatest sea ice TCO_2 losses occurred on 15-16 January during initial sea ice growth and from 23 to 25 January, during ice cooling due to snow removal. The exchange of CO_2 between the ice and the atmosphere is known (Fig. 5). The number of mole of CO_2 exchanges between the ice and the atmosphere were calculated (noted as $CO_{2(air\text{-}ice)}$ in Table 2) using the time step between each flux measurement, the ice thickness and density. During sea ice growth 0.01 to 0.42 mol of CO_2 were released from the ice-covered pool to the atmosphere. During sea ice melt uptake of atmospheric CO_2 by the ice-covered pool ranged from -0.15 to -0.93 (Fig. 9, white triangles). On average, over the duration of the experiment, the ice cover released 0.08 mol of CO_2 to the atmosphere. Assuming we know how much ikaite is contained within the ice cover (Fig. 8b), we can estimate how much TCO_2 is exported from the ice to the underlying seawater (Fig. 9, blue triangles) by subtracting the air-ice CO_2 exchange and the ikaite precipitation from the total reduction of $TCO_{2(ice)}$ observed within the ice cover (Fig. 9, black dots). The sea ice-to-seawater TCO_2 export ranged from 0.2 to 3.98 mol (average = 1.7 mol), confirming that sea ice primarily exports TCO_2 to the underlying seawater. TCO_2 export from the ice to the water column ranged from 23% of the total sea ice TCO_2 early in the ice growth (14 January) to 100% after the onset of melt. These estimations are comparable to the study of Sejr et al., (2011) who suggested that sea ice exports 99% of its total TCO_2 to the seawater below it. On average over the whole experiment, sea ice exported 1.7 mol of TCO_2 to the underlying seawater (Fig. 9), which corresponds to a $TCO_{2(sw)}$ increase of 43.5 µmol kg^{-1} considering the average sea ice thickness and density during the experiment and the volume of the pool. However, $TCO_{2(sw)}$ increased by 115 µmol kg^{-1} over the whole experiment (Fig. 3b), leaving an increase of 71.5 µmol kg^{-1} in the $TCO_{2(sw)}$ that cannot be explained by the sea ice-seawater exchange of TCO_2. We

postulate that as the ice melt advanced, patches of open water that opened at the surface of the pool which were undersaturated compared to the atmosphere (Fig. 3d) imported the additional TCO_2 directly from the atmosphere in the form of $CO_{2(g)}$. Considering the pool volume, the 71.5 µmol kg^{-1} increase of $TCO_{2(sw)}$ could be explained by an air-sea water CO_2 uptake of 8.5 mmol m^{-2} d^{-1} over 3 days of sea ice melt in a 20% ice free pool. High air-sea gas exchanges rates have been observed over partially ice-covered seas (Else et al., 2011; 2013). This mechanism is also corroborated by models that account for additional sources of turbulence generated by the presence of sea ice (Loose et al., 2014).

The design of the experiment allowed for constrained measurements of inorganic carbon fluxes between sea ice and the water column not possible in a natural environment where large volume, mixing processes alter the underlying seawater making it more complicated to identify changes. We build a CO_2 budget based only on the sea ice growth phase because only two days of data for the melt phase are available and the experiment stopped while the pool was 20% ice-free (Rysgaard et al., 2014; Else et al., 2015). The initial seawater (origin point, t=0) contained 1040.9 mol of $TCO_{2(sw)}$ on 11 January while on the last day of sea ice growth (25 January) the seawater contained 1017.3 mol of $TCO_{2(sw)}$ (Table 2) with the difference, (23.6 mol of TCO_2) in all likelihood transferred from the water column to the ice cover or the atmosphere. However, the TCO_2 content within the ice cover at the end of the growing phase was 15.6 mol and the ice cover released 3.1 mol of CO_2 to the atmosphere (Table 2). Therefore, 4.9 mol of the 23.6 mol of TCO_2 exchanged from the water column are unaccounted for, but may be explained by air-ice CO_2 fluxes. The chamber measurement technique for air-ice CO_2 flux may underestimate the exchange of CO_2, and the air-seawater CO_2 fluxes are unknown until the ice started to grow (13 January). These missing moles of TCO_2 may also be explained by our assumption of uniform sea ice thickness in the SERF. Using the seawater conditions at the end of the experiment, 1-cm of seawater in the pool contains 4.21 mol of TCO_2, making it difficult to close our budget.

5.5. Potential impact of sea ice growth and ikaite export on aragonite saturation state of the underlying seawater.

The Arctic Ocean is a region where calcifying organisms are particularly vulnerable to ocean acidification since low temperatures and low salinity lower the carbonate saturation state. As a result several areas of the Arctic Ocean are already undersaturated with respect to aragonite (Chierici and Fransson 2009; Yamamoto-Kawai et al., 2009; Bates et al., 2011). This undersaturation is enhanced in winter as the temperature decreases and pCO_2 increases as a result of respiration. Calcifying organisms

might therefore be most susceptible to the effects of acidification in the winter, corresponding to the annual minimum in aragonite saturation state ($\Omega_{aragonite}$). Sea ice retreat is thought to enhance the impact of ocean acidification by freshening and ventilating the surface water (Yamamoto-Kawai et al., 2008; Yamamoto et al., 2012; Popova et al., 2014). However, any understanding of the effect of ikaite precipitation in sea ice on ocean acidification is still in its infancy (e.g. Fransson et al., 2013).

Since the discovery of ikaite precipitation in sea ice (Dieckmann et al., 2008), research on its impact on the carbonate system of the underlying seawater has been ongoing. Depending on the timing and location of this precipitation within sea ice, the impact for the atmosphere and the water column in terms of CO_2 transport can be significantly different (Delille et al., 2014). Dissolution of ikaite within melting sea ice in the spring and export of this related high TA:TCO_2 ratio meltwater from the ice to the water column will decrease the pCO_2, increase pH and $\Omega_{aragonite}$ of the surface layer seawater. Accordingly, during sea ice melt, an increase of $\Omega_{aragonite}$ in the surface water in the Arctic was observed (Chierici et al., 2011, Fransson et al., 2013, Bates et al., 2014). However, it was difficult to ascribe this increase to the legacy of excess TA in sea ice, ikaite dissolution or primary production.

The impact of ikaite precipitation on the surface seawater during sea ice growth is less clear. Fransson et al., (2013) suggested in winter in the Amundsen Gulf that the release of brine decreased $\Omega_{aragonite}$ by 0.8 at the sea ice-seawater interface as a result of ikaite precipitation within sea ice and the related CO_2 enrichment of brine. Conversely, during ice melt, $\Omega_{aragonite}$ increased by 1.4 between March and May, likely due to both calcium carbonate dissolution and primary production. This contrasts with the present experiment. Figure 10 shows the evolution of $\Omega_{aragonite}$ and pH in the water column derived from $TA_{(sw)}$ and $TCO_{2(sw)}$ and the evolution of $\Omega_{aragonite}$ and pH predicted solely from salinity changes (i.e. using $TA_{(sw)}^{*}$ and $TCO_{2(sw)}^{*}$, noted as $\Omega_{aragonite}^{*}$ and pH^{*}). We used the CO2sys_v2.1.xls spreadsheet (Pierrot et al., 2006) with the dissociation constants from Goyet and Dickson (1989) and all other constants from DOE (1994). This shows the complexity of ikaite and its impact on the carbonate system and Ω in the underlying water.

During ice growth, sea ice brine rejection appears to increase both pH (from 8.00 to 8.06) and $\Omega_{aragonite}$ (from 1.28 to 1.65) of the underlying seawater, offsetting the effect of decreased temperature. A slight increase of $\Omega_{aragonite}$ was predicted due to increased salinity and a proportional increase of TA and TCO_2 as depicted in $\Omega_{aragonite}^{*}$. However, the effect of ikaite rejection and subsequent changes in TA strongly enhance the increase of $\Omega_{aragonite}$. Therefore, ikaite rejection from sea ice has a much stronger potential to

increase $\Omega_{aragonite}$ than brine rejection during fall and winter sea ice growth, suggesting ikaite exported to seawater from sea ice may hamper the effect of oceanic acidification on $\Omega_{aragonite}$ in fall and winter in at the time when $\Omega_{aragonite}$ is at its minimum (Chierici and Fransson 2009, Yamamoto-Kawai et al., 2009, Chierici et al., 2011). Ice formation may therefore delay harmful effects of ocean acidification on calcifying organisms by increasing $\Omega_{aragonite}$ in the critical winter period when $\Omega_{aragonite}$ reaches its minimal values. As a corollary, ice removal acts to alleviate the effect of ikaite rejection and may therefore lowers $\Omega_{aragonite.}$ This calls for an accounting of under-ice ikaite rejection in modeling predictions on the consequences of Arctic Ocean acidification in the context of northern hemispheric annual multi-year sea ice loss, as increased summer open water will lead to more first year sea ice formation in fall and winter in the future.

6. Conclusion

We quantified the evolution of inorganic carbon dynamics from initial sea ice formation to its melt in a sea ice-seawater mesocosm pool from 11 to 29 January 2013. Based on our analysis of TA and TCO_2 in sea ice and seawater, the main processes affecting inorganic carbon within sea ice are ikaite precipitation and CO_2 exchange with the atmosphere, while in the underlying seawater dissolution of ikaite was the main process affecting the inorganic carbon system.

During this experiment, sea ice exchanged inorganic carbon components (e.g. CO_2, ikaite, TCO_2) with both the atmosphere and the underlying seawater. During sea ice growth, CO_2 was released to the atmosphere while during ice melt an uptake of atmospheric CO_2 was observed. We report ikaite precipitation up to 167 µmol kg^{-1} of sea ice, similar to previous estimates from Rysgaard et al., (2014) based on microscopically observed values. In the underlying seawater, a net increase of $nTA_{(sw)}$ over the whole experiment was observed (up to 128 µmol kg^{-1}), suggesting that a portion of the ikaite crystals precipitated within sea ice were exported to the underlying seawater and then dissolved as the ice cover evolved in time. Ikaite export from ice to the underlying seawater was associated with brine rejection during sea ice growth, increased sea ice vertical connectivity due to the upward percolation of seawater, and meltwater flushing during sea ice melt. Rysgaard et al., (2007) suggested that ikaite precipitation within sea ice could act as a significant sink for atmospheric CO_2, however to act as a sink for atmospheric CO_2, ikaite crystals must remain in the ice structure while the CO_2 produced by their precipitation is expelled with dense brine rejection and entrained in deep seawater (Delille et al., 2014). TA changes observed in the water column once the sea ice started to melt indicate that more than half of

559 the total amount of ikaite precipitated in the ice during the sea ice growth remained in the ice until the sea
560 ice began to melt. Derivation of air-sea CO_2 fluxes related to the sea ice carbon pump should take into
561 account ikaite export to the underlying ocean during sea ice growth, which might reduce the efficiency of
562 oceanic CO_2 uptake upon sea ice melt. As sea ice melts, ikaite is flushed downward out of the ice along
563 with the meltwater.

564 Ikaite export from sea ice and its dissolution had a strong impact on the underlying seawater. In this
565 semi-closed system, sea ice growth increased the seawater salinity, $TA_{(sw)}$, and $TCO_{2(sw)}$. In spite of those
566 increases, the pCO_2 of the underlying seawater remained undersaturated compared to the atmosphere. We
567 conclude that ikaite dissolution within the water column is responsible for the seawaters' continual pCO_2
568 undersaturation. In addition, we discuss that dissolution of ikaite crystals exported from sea ice in the
569 underlying seawater can potentially hamper the effect of oceanic acidification on $\Omega_{aragonite}$ in fall and
570 winter in ice-covered areas at the time when $\Omega_{aragonite}$ is smallest.

571 **7. Acknowledgments**

572 We gratefully acknowledge the contributions of the Canada Excellence Research Chair (CERC) and
573 Canada Research Chair (CRC) programs. Support was also provided by the Natural Sciences and
574 Engineering Research Council (NSERC), the Canada Foundation for Innovation and the University of
575 Manitoba. RJG thanks the NSERC Discovery Grant program. B.D. is a research associate researcher of
576 the F.R.S.-FNRS. This work is a contribution to the ArcticNet Networks of Centre of Excellence
577 and the Arctic Science Partnership (ASP) asp-net.org and the ARC-cake club. The authors are grateful to
578 the anonymous reviewers and to the editor whose comments greatly improved the quality of the
579 manuscript.

580 **8. References**

581 Bates, N. R., Cai, W. J., and Mathis, J. T.: The ocean carbon cycle in the western Arctic Ocean: Distributions
582 and air-sea fluxes of carbon dioxide, Oceanography, 24, 186-201, 2011.

583 Bates, N. R. and Mathis, J. T.: The Arctic Ocean marine carbon cycle: evaluation of air-sea CO_2 exchanges,
584 ocean acidification impacts and potential feedbacks, Biogeosciences, 6, 2433-2459, 2009.

585 Bates, N. R., Garley, R., Frey, K. E., Shake, K. L., Mathis, J. L.: Sea-ice melt CO_2-carbonate chemistry in the
586 western Arctic Ocean: meltwater contribution to air-sea CO_2 gas exchange, mixed-layer properties and rates of
587 net community production under sea ice, Biogeosciences, 11, 6769-6789, doi:10.5194/bg-11-6769-2014, 2014.

588 Chierici, M. and Fransson, A.: Calcium carbonate saturation in the surface water of the Arctic Ocean:
589 undersaturation in freshwater influenced shelves, Biogeosciences, 6, 2421-2431, 2009.

590 Chierici, M., Fransson, A., Lansard, B., Miller, L. A., Mucci, A., Shadwick, E., Thomas, E., Tremblay, J. E. and
591 Papakyriakou, T.: The impact of biogeochemical processes and environmental factors on the calcium carbonate
592 saturation state in the Circumpolar Flaw Lead in the Amundsen Gulf, Arctic Ocean, Journal of Geophysical
593 Research-Oceans, 116, C00G09, doi:10.1029/2011JC007184, 2011.

594 Copin Montégut, C.: A new formula for the effect of temperature on the partial pressure of carbon dioxide in
595 seawater, Marine Chemistry, 25, 29-37, 1988.

596 Cox, G. F. N. and Weeks, W. F.: Equations for determining the gas and brine volumes in sea-ice samples,
597 Journal of Glaciology, 29, 306 - 316, 1983.

598 Delille, B., Vancoppenolle, M., Geilfus, N.-X., Tilbrook, B., Lannuzel, D., Schoemann, V., Becquevort, S.,
599 Carnat, G., Delille, D., Lancelot, C., Chou, L., Dieckmann, G. S., and Tison, J.-L.: Southern Ocean CO_2 sink:
600 The contribution of the sea ice, Journal of Geophysical Research: Oceans, 119, 6340-6355, 2014.

601 Dieckmann, G. S., Nehrke, G., Papadimitriou, S., Gottlicher, J., Steininger, R., Kennedy, H., Wolf-Gladrow, D.,
602 and Thomas, D. N.: Calcium carbonate as ikaite crystals in Antarctic sea ice, Geophysical Research Letters, 35,
603 2008.

604 DOE (Ed.): Handbook of methods for the analysis of the various parameters of the carbon dioxide system in sea
605 water, 1994.

606 Ducklow, H. W.: Seasonal production and bacterial utilization of DOC in the Ross Sea, Antarctica, Biogeochem.
607 Ross Sea, vol 78, 143-158, 2003.

608 Else, B. G. T., Galley, R. J., Lansard, B., Barber, D. G., Brown, K., Miller, L. A., Mucci, A., Papakyriakou, T.
609 N., Tremblay, J. E., and Rysgaard, S.: Further observations of a decreasing atmospheric CO_2 uptake capacity in
610 the Canada Basin (Arctic Ocean) due to sea ice loss, Geophysical Research Letters, 40, 1132-1137, 2013.

611 Else, B. G. T., Papakyriakou, T., Galley, R., Drennan, W. M., Miller, L. A., and Thomas, H.: Wintertime CO_2
612 fluxes in an Arctic polynya using eddy covariance: Evidence for enhanced air-gas transfer during ice formation,
613 Journal of Geophysical Research, 116, 2011.

614 Else, B. G. T., Rysgaard, S., Attard, K., Campbell, K., Crabeck, O., Galley, R. J., Geilfus, N. X., Lemes, M.,
615 Lueck, R., Papakyriakou, T., and Wang, F.: Under-ice eddy covariance flux measurements of heat, salt,

momentum, and dissolved oxygen in an artificial sea ice pool, Cold Regions Science and Technology, 119, 158-169, 2015.

Frankignoulle, M.: Field-Measurements of Air Sea CO_2 Exchange, Limnology and Oceanography, 33, 313-322, 1988.

Fransson, A., Chierici, M., Miller L. A., Carnat G., Shadwick, E., Thomas, H., Pineault, S. and Papakyriakou, T. N.: Impact of sea-ice processes on the carbonate system and ocean acidification at the ice-water interface of the Amundsen Gulf, Arctic Ocean, Journal of Geophysical Research: Oceans, 118, 7001-7023, 2013.

Galley, R. J., Else, B. G. T., Geilfus, N. X., Hare, A. A., Isleifson, D., Barber, D. G., and Rysgaard, S.: Imaged brine inclusions in young sea ice-Shape, distribution and formation timing, Cold Regions Science and Technology, 111, 39-48, 2015.

Garneau, M. E., Vincent, W. F., Alonso-Sáez L., Gratton, Y., Lovejoy, C.:Prokaryotic community structure and heterotrophic production in a river-influenced coastal arctic ecosystem, Aquat. Microb. Ecol., 32, 27-40, 2006.

Geilfus, N. X., Carnat, G., Dieckmann, G. S., Halden, N., Nehrke, G., Papakyriakou, T., Tison, J. L., and Delille, B.: First estimates of the contribution of $CaCO_3$ precipitation to the release of CO_2 to the atmosphere during young sea ice growth, Journal of Geophysical Research, 118, 2013a.

Geilfus, N. X., Carnat, G., Papakyriakou, T., Tison, J. L., Else, B., Thomas, H., Shadwick, E., and Delille, B.: Dynamics of pCO_2 and related air-ice CO_2 fluxes in the Arctic coastal zone (Amundsen Gulf, Beaufort Sea), Journal of Geophysical Research-Oceans, 117, 2012.

Geilfus, N. X., Galley, R. J., Cooper, M., Halden, N., Hare, A., Wang, F., Søgaard, D. H., and Rysgaard, S.: Gypsum crystals observed in experimental and natural sea ice, Geophysical Research Letters, doi: 10.1002/2013GL058479, 2013b. 2013GL058479, 2013b.

Geilfus, N. X., Galley, R. J., Crabeck, O., Papakyriakou, T., Landy, J., Tison, J. L., and Rysgaard, S.: Inorganic carbon dynamics of melt-pond-covered first-year sea ice in the Canadian Arctic, Biogeosciences, 12, 2047-2061, 2015.

Geilfus, N. X., Tison, J. L., Ackley, S. F., Galley, R. J., Rysgaard, S., Miller, L. A., and Delille, B.: Sea ice pCO_2 dynamics and air-ice CO_2 fluxes during the Sea Ice Mass Balance in the Antarctic (SIMBA) experiment - Bellingshausen Sea, Antarctica, The Cryosphere, 8, 2395-2407, 2014.

643 Golden, K. M., Eicken, H., Heaton, A. L., Miner, J., Pringle, D. J., and Zhu, J.: Thermal evolution of
644 permeability and microstructure in sea ice, Geophysical Research Letters, 34, 2007.

645 Goyet, C. and Poisson, A.: New determination of carbonic acid dissociation constants in seawater as a function
646 of temperature and salinity, Deep-Sea Research Part a-Oceanographic Research Papers, 36, 1635-1654, 1989.

647 Grasshoff, K., Ehrhardt, M., and Kremling, K.: Methods of sea water analysis, Verlag Chemie, 1983. 1983.

648 Hansen, J. W., Thamdrup, B., and Jørgensen, B. B.: Anoxic incubation of sediment in gas-tight plastic bags: a
649 method for biogeochemical processes studies, Marine Ecology-Progress Series, 208, 273-282, 2000.

650 Haraldsson, C., Anderson, L. G., Hassellov, M., Hulth, S., and Olsson, K.: Rapid, high-precision potentiometric
651 titration of alkalinity in ocean and sediment pore waters, Deep sea Research I, 44, 2031-2044, 1997.

652 Hare, A. A., Wang, F., Barber, D., Geilfus, N. X., Galley, R. J., and Rysgaard, S.: pH Evolution in sea ice grown
653 at an outdoor experimental facility, Marine Chemistry, 154, 46-54, 2013.

654 Johnson, K. M., Sieburth, J. M., Williams, P. J. L., and Brandstrom, L.: Coulometric total carbon-dioxide
655 analysis for marine studies – automation and calibration, Marine Chemistry, 21, 117-133, 1987.

656 Killawee, J. A., Fairchild, I. J., Tison, J. L., Janssens, L., and Lorrain, R.: Segregation of solutes and gases in
657 experimental freezing of dilute solutions: Implications for natural glacial systems, Geochimica Et Cosmochimica
658 Acta, 62, 3637-3655, 1998.

659 Kirchmann, D. L.: Leucine incorporation as a measure of biomass production by heterotrophic bacteria.
660 Handbook of Methods in Aquatic Microbial Ecology, Chap. 58, 509-518, 1993.

661 Kirchmann, D. L.: Measuring bacterial biomass production and growth rates from Leucine incorporation in
662 natural aquatic environments. Methods in Microbiology, Chap. 12, 227-237, 2001.

663 Leppäranta, M. and Manninen, T.: The brine and gas content of sea ice with attention to low salinities and high
664 temperatures, Helsinki, 1988.

665 Loose, B., McGillis, W. R., Perovich, D., Zappa, C. J., and Schlosser, P.: A parameter model of gas exchange for
666 the seasonal sea ice zone, Ocean Science, 10, 17-28, 2014.

667 MacGilchrist, G. A., Garabato, A. C. N., Tsubouchi, T., Bacon, S., Torres-Valdes, S., and Azetsu-Scott, K.: The
668 Arctic Ocean carbon sink, Deep-Sea Research Part I-Oceanographic Research Papers, 86, 39-55, 2014.

669 Miller, L. A., Papakyriakou, T., Collins, R. E., Deming, J., Ehn, J., Macdonald, R. W., Mucci, A., Owens, O.,
670 Raudsepp, M., and Sutherland, N.: Carbon Dynamics in Sea Ice: A Winter Flux Time Series, Journal of
671 Geophysical Research-Oceans, 116, 2011.

672 Nomura, D., Eicken, H., Gradinger, R., and Shirasawa, K.: Rapid physically driven inversion of the air-sea ice
673 CO_2 flux in the seasonal landfast ice off Barrow, Alaska after onset surface melt, Continental Shelf Research, 30,
674 1998-2004, 2010.

675 Nomura, D., Granskog, M. A., Assmy, P., Simizu, D., and Hashida, G.: Arctic and Antarctic sea ice acts as a
676 sink for atmospheric CO_2 during periods of snowmelt and surface flooding, Journal of Geophysical Research:
677 Oceans, doi: 10.1002/2013JC009048, 2013. 6511-6524, 2013.

678 Parsons T. R., Maita Y., Lali C. M.: A manual of chemical and biological methods for seawater analysis.
679 Pergamon Press, Toronto, 1984

680 Papadimitriou, S., Kennedy, H., Kattner, G., Dieckmann, G. S., and Thomas, D. N.: Experimental evidence for
681 carbonate precipitation and CO_2 degassing during sea ice formation, Geochimica et Cosmochimica Acta, 68,
682 1749-1761, 2004.

683 Papakyriakou, T. and Miller, L.: Springtime CO_2 exchange over seasonal sea ice in the Canadian Arctic
684 Archipelago, Annals of Glaciology, 52, 2011.

685 Parmentier, F.-J. W., Christensen, T. R., Sørensen, L. L., Rysgaard, S., McGuire, A. D., Miller, P. A., and
686 Walker, D. A.: The impact of lower sea-ice extent on Arctic greenhouse-gas exchange, Nature climate change,
687 doi: DOI:10.1038/NCLIMATE1784, 2013. 195-202, 2013.

688 Pierrot, D., Lewis, E., and Wallace, D. W. R.: MS Excel Program Developed for CO_2 System Calculations,
689 Carbon Dioxide Information Analysis Center, Oak Ridge National Laboratory, U.S. Department of Energy, Oak
690 Ridge, Tennessee, doi: 10.3334/CDIAC/otg.CO2SYS_XLS_CDIAC105a, 2006. ORNL/CDIAC-105a. , 2006.

691 Popova, E. E., Yool, A., Aksenov, Y., Coward, A. C., and Anderson, T. R.: Regional variability of acidification
692 in the Arctic: a sea of contrasts, Biogeosciences, 11, 293-308, 2014.

693 Rysgaard, S., Bendtsen, J., Pedersen, L. T., Ramlov, H., and Glud, R. N.: Increased CO_2 uptake due to sea ice
694 growth and decay in the Nordic Seas, Journal of Geophysical Research, 114, 2009.

695 Rysgaard, S., Glud, R. N., Sejr, M. K., Bendtsen, J., and Christensen, P. B.: Inorganic carbon transport during
696 sea ice growth and decay: A carbon pump in polar seas, Journal of Geophysical Research-Oceans, 112, 2007.

Rysgaard, S., Søgaard, D. H., Cooper, M., Pu, cacute, ko, M., Lennert, K., Papakyriakou, T. N., Wang, F., Geilfus, N. X., Glud, R. N., Ehn, J., McGinnis, D. F., Attard, K., Sievers, J., Deming, J. W., and Barber, D.: Ikaite crystal distribution in winter sea ice and implications for CO_2 system dynamics, The Cryosphere, 7, 707-718, 2013.

Rysgaard, S., Wang, F., Galley, R. J., Grimm, R., Notz, D., Lemes, M., Geilfus, N. X., Chaulk, A., Hare, A. A., Crabeck, O., Else, B. G. T., Campbell, K., Sørensen, L. L., Sievers, J., and Papakyriakou, T.: Temporal dynamics of ikaite in experimental sea ice, The Cryosphere, 8, 1469-1478, 2014.

Sabine, C. L., Feely, R. A., Gruber, N., Key, R. M., Lee, K., Bullister, J. L., Wanninkhof, R., Wong, C. S., Wallace, D. W. R., Tilbrook, B., Millero, F. J., Peng, T. H., Kozyr, A., Ono, T., and Rios, A. F.: The oceanic sink for anthropogenic CO_2, Science, 305, 367-371, 2004.

Sejr, M. K., Krause-Jensen, D., Rysgaard, S., Sorensen, L. L., Christensen, P. B., and Glud, R. N.: Air-sea flux of CO_2 in arctic coastal waters influenced by glacial melt water and sea ice, Tellus Series B Chemical and Physical Meteorology, 63, 815-822, 2011.

Semiletov, I. P., Makshtas, A., Akasofu, S. I., and Andreas, E. L.: Atmospheric CO_2 balance: The role of Arctic sea ice, Geophysical Research Letters, 31, 2004.

Søgaard, D. H., Thomas, D. N, Rysgaard, S., Norman, L., Kaartokallio, H., Juul-Pedersen T., Glud, R. N. and Geilfus, N. X.: The relative contributions of biological and abiotic processes to the carbon dynamics in subarctic sea ice, Polar Biol., doi:10.1007/s00300-013-1396-3, 2013.

Yamamoto, A., Kawamiya, M., Ishida, A., Yamanaka, Y., and Watanabe, S.: Impact of rapid sea-ice reduction in the Arctic Ocean on the rate of ocean acidification, Biogeosciences, 9, 2365-2375, 2012.

Yamamoto-Kawai, M., McLaughlin, F. A., Carmack, E. C., Nishino, S., and Shimada, K.: Aragonite Undersaturation in the Arctic Ocean: Effects of Ocean Acidification and Sea Ice Melt, Science, 326, 1098-1100, 2009.

Yamamoto-Kawai, M., McLaughlin, F. A., Carmack, E. C., Nishino, S., and Shimada, K.: Freshwater budget of the Canada Basin, Arctic Ocean, from salinity, delta O-18, and nutrients, Journal of Geophysical Research-Oceans, 113, 12, 2008.

Zeebe, R. E. and Wolf-Gladrow, D.: CO_2 in seawater: Equilibrium, Kinetics, Isotopes, Elsevier, 2001. 2001.

9. Table

Table 1: Seawater conditions on 11 January, before any sea ice formation (t=0), on 25 January, just before the heat was turned back on and on 29 January, at the end of the experiment. Note that seawater salinity and $TA_{(sw)}$ do not reach the initial seawater values as sea ice was still present at the end of the experiment.

Date	Temperature (°C)	Salinity	TA (µmol kg^{-1})	*n*TA (µmol kg^{-1})	TCO_2 (µmol kg^{-1})	$nTCO_2$ (µmol kg^{-1})
11 Jan.	-1.4	33.5	2453	2416	2341	2306
25 Jan.	-1.9	35.5	2659	2471	2524	2346
29 Jan.	-0.6	34.4	2607	2500	2461	2361

732 Table 2: Masses of TCO_2 in the water column ($TCO_{2(sw)}$) and in the ice cover ($TCO_{2(ice)}$), masses of
733 ikaite within the ice cover estimated from this study and from Rysgaard et al., (2014), masses
734 of ikaite dissolved in the water column ($Ikaite_{(sw)}$) and masses of CO_2 exchanged between the
735 ice and the atmosphere over the whole pool (estimation based on the air-ice CO_2 fluxes). All
736 units are in mole.

January (DOY)	$TCO_{2(sw)}$	$TCO_{2(ice)}$	$Ikaite_{(ice)}$ *from this study*	$Ikaite_{(ice)}$ *from Rysgaard et al., (2014)*	$Ikaite_{(sw)}$	$CO_{2(air-ice)}$
t=0	1041					
13.75	1040	2.38	0.17	0.00	0.47	
13.88	1044	2.09	0.00	0.00	0.87	
14	1043	2.90	0.25	0.00	0.83	0.03
14.13	1043	3.29	0.62	0.00	2.57	0.02
14.25	1038	4.91	-0.05	0.00	1.06	0.01
14.5	1037	4.77	0.18	0.00	3.75	0.12
14.75	1039	4.36	0.12	0.05	2.73	0.07
15	1037				1.80	0.08
15.25	1032	4.67	0.98	0.68	1.28	0.01
15.5	1034	3.89	1.58	0.00	-1.57	0.07
15.92	1034	4.47	0.69	0.00	1.63	0.12
16.38	1024	7.36	1.45	0.08	3.60	0.19
16.67	1028	8.17	1.87	0.00	6.00	0.10
17.38	1023	15.48	0.29	0.65	3.90	0.22
17.67	1026	13.26	0.04	0.46	4.50	0.13
18.38	1030	11.39	0.74	2.14	5.61	0.38
18.67	1027	12.06	0.21	0.21	7.16	0.10
19.38	1029	11.13	0.01	0.84	6.96	0.23
19.67	1030	10.75	0.03	0.09	1.97	0.11
20.38	1028	10.25	-0.12	0.23	1.47	0.42
20.67	1022	10.36	-0.70	0.71	3.48	0.12
21.38	1025	10.50	0.88	0.35	7.42	0.35
23.63	1034	12.60	1.34	2.14	11.18	
24.38	1026	14.84	1.30	1.94	9.75	0.21
25.38	1017	15.67	1.09	3.05	6.62	
25.5	1029				11.51	0.02
28.67	1022	13.46	-0.57	0.46	20.91	-0.93
29.38	987.3	15.82	-0.56	0.55	26.72	-0.15

737

10. Figure Captions

Figure 1: The Sea Ice Environmental Research Facility with thin sea ice covering the pond during the 2013 experiment. Photo: J. Sievers.

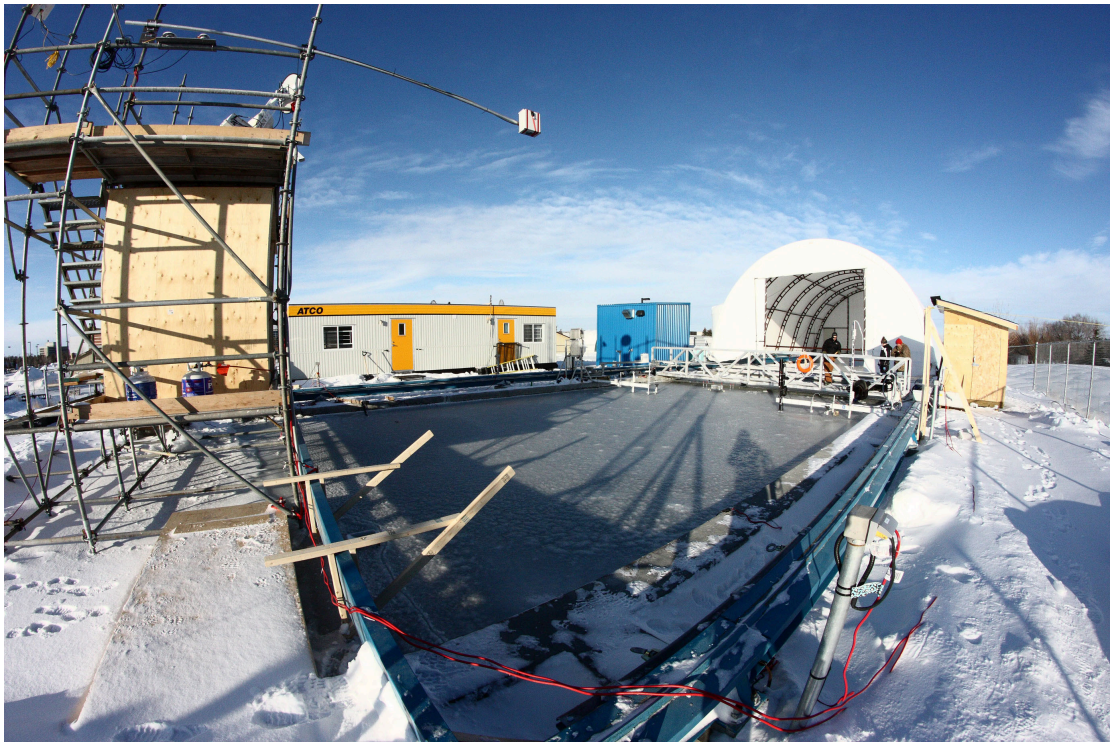

Figure 2: Evolution of (**a**) Air temperature (°C) at 2 m height, (**b**) snow thickness (black shaded areas) and sea ice/seawater temperature (°C), (**c**) bulk ice salinity, (**d**) brine volume content within sea ice, (**e**) seawater temperature (blue) and salinity (green). Measurements were performed at 30, 100, 175 and 245 cm water depths. The darker the color is, the closer to the surface. In panels (**b**), (**c**), (**d**) sea ice thickness is illustrated by black dots. Stars on panel (**b**) represent the depth at which the temperature profiles are derived from. Open squares in the lower part of (**d**) mark the sampling times. The dashed line on panel (e) indicates when the heat at the bottom of the pool was turned back on.

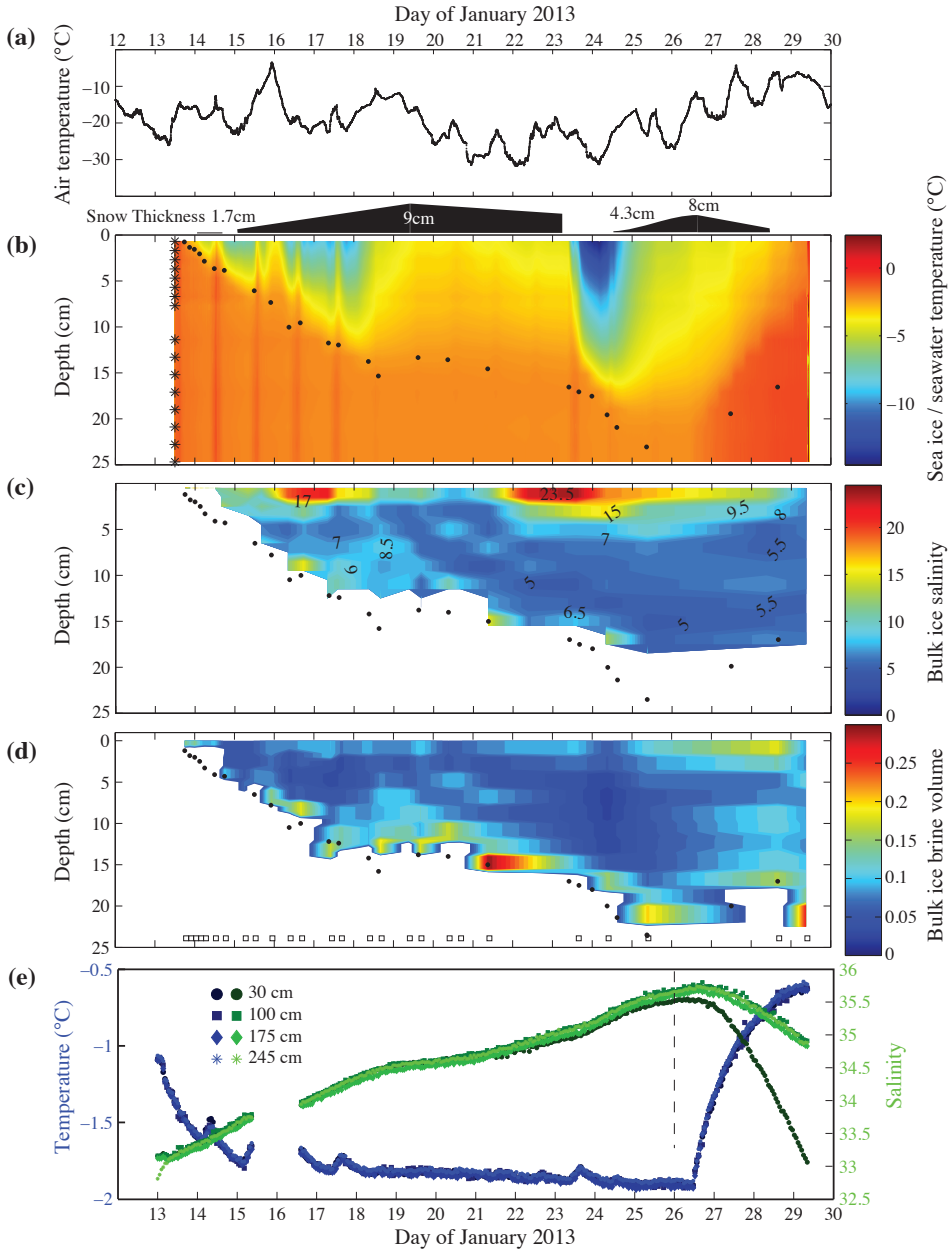

Figure 3: Evolution of (**a**) $TA_{(sw)}$ and $TA_{(sw)}^{*}$(µmol kg^{-1}), (**b**) $TCO_{2(sw)}$ and $TCO_{2(sw)}^{*}$ (µmol kg^{-1}), (**c**) $nTA_{(sw)}$ (black) and $nTCO_{2(sw)}$ (green) (µmol kg^{-1}) and (**d**) the seawater pCO_2 (µatm) measured in situ (black) and corrected to a constant temperature of -1°C (blue). In panels (**a**) and (**b**) the black line is the average over the three depths while the dotted red line is the expected concentrations according to the variation of salinity observed and calculated from the mean values of the three depths ($TA_{(sw)}^{*}$ and $TCO_{2(sw)}^{*}$, respectively). The vertical black dotted line on 26 January mark when the heat was turned back ON.

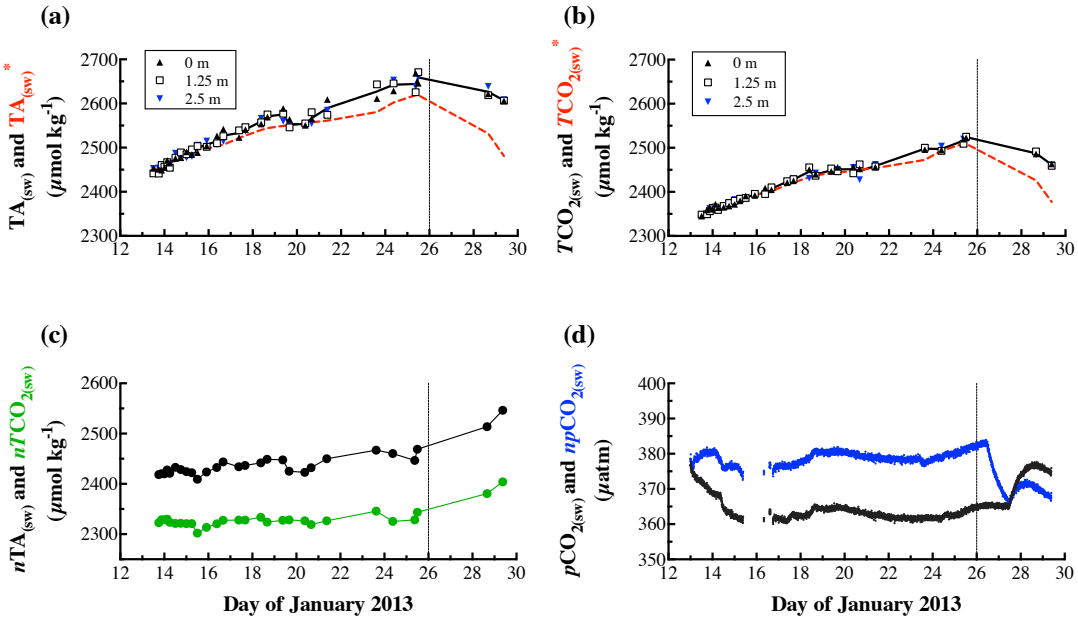

Figure 4: Evolution of (**a**) $TA_{(ice)}$ (µmol kg^{-1}), (**b**) $TCO_{2(ice)}$ (µmol kg^{-1}), (**c**) $nTA_{(ice)}$ (µmol kg^{-1}) and (**d**) $nTCO_{2(sw)}$ (µmol kg^{-1}). Sea ice thickness is illustrated by black dots. Open squares in the lower part of (**d**) mark the sampling times.

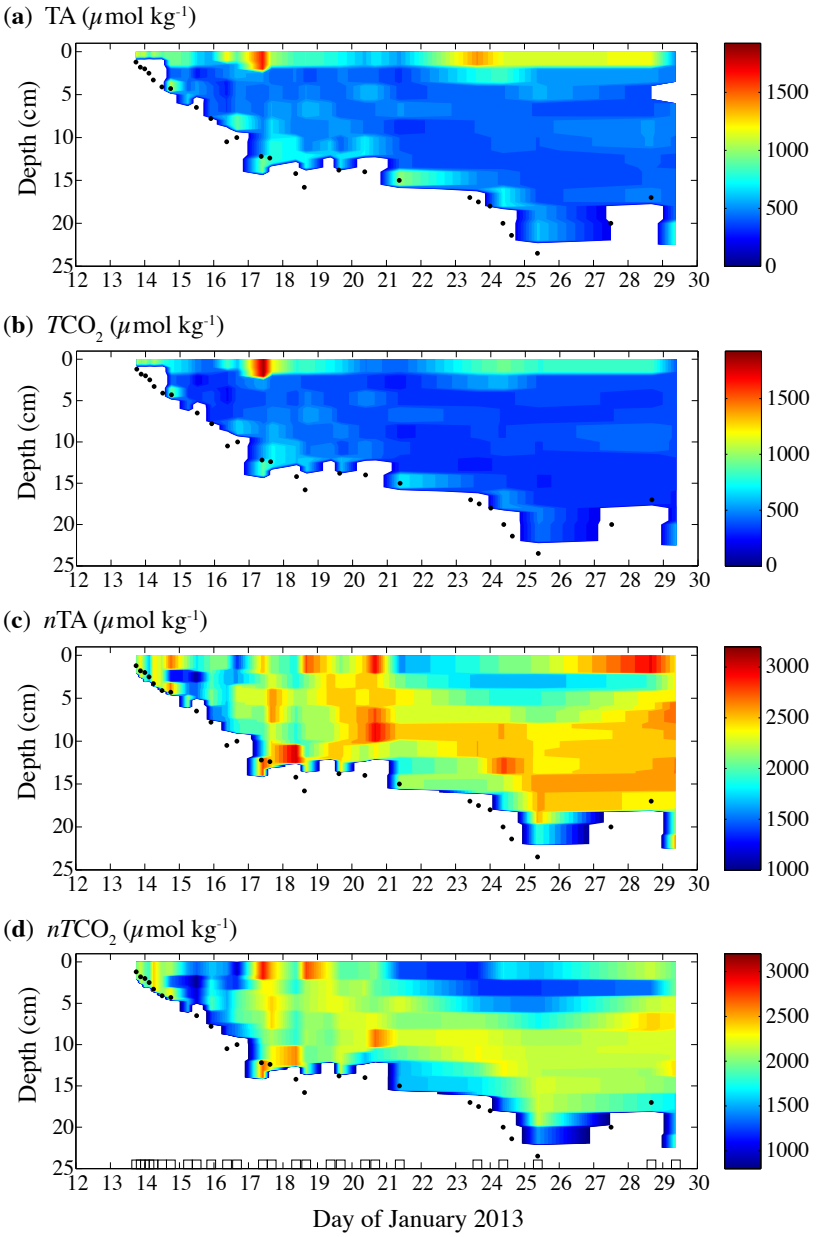

Figure 5: Air-ice CO_2 fluxes (mmol m^{-2} d^{-1}). Positive air-ice CO_2 flux means outgassing from the ice and negative CO_2 flux means uptake of atmospheric CO_2. The vertical black dotted line on 26 January mark when the heat was turned back ON.

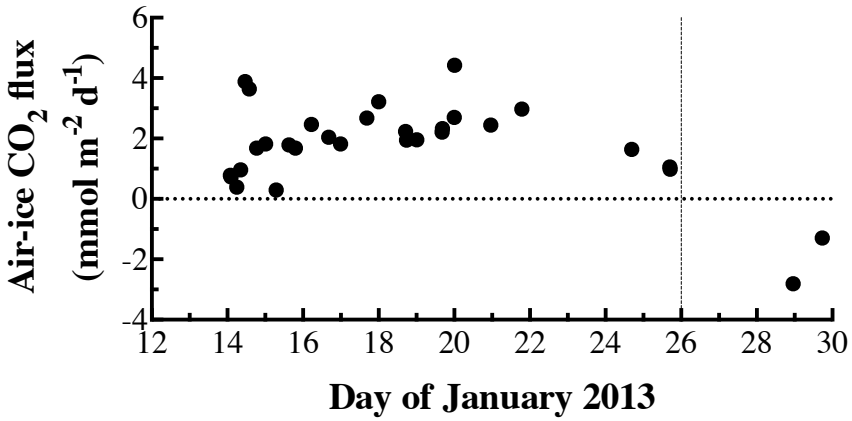

Figure 6: (**a**) Relationship between $nTCO_2$ and nTA (µmol kg^{-1}) in bulk sea ice (white hexagons) and seawater (black dots), (**b**) Zoom on seawater data. The different dotted lines represent the theoretical evolution of nTA and $nTCO_2$ ratio following the precipitation/dissolution of calcium carbonate and release/uptake of $CO_{2(g)}$. A linear regression is shown in green for the ice samples (a) and blue for seawater samples (b).

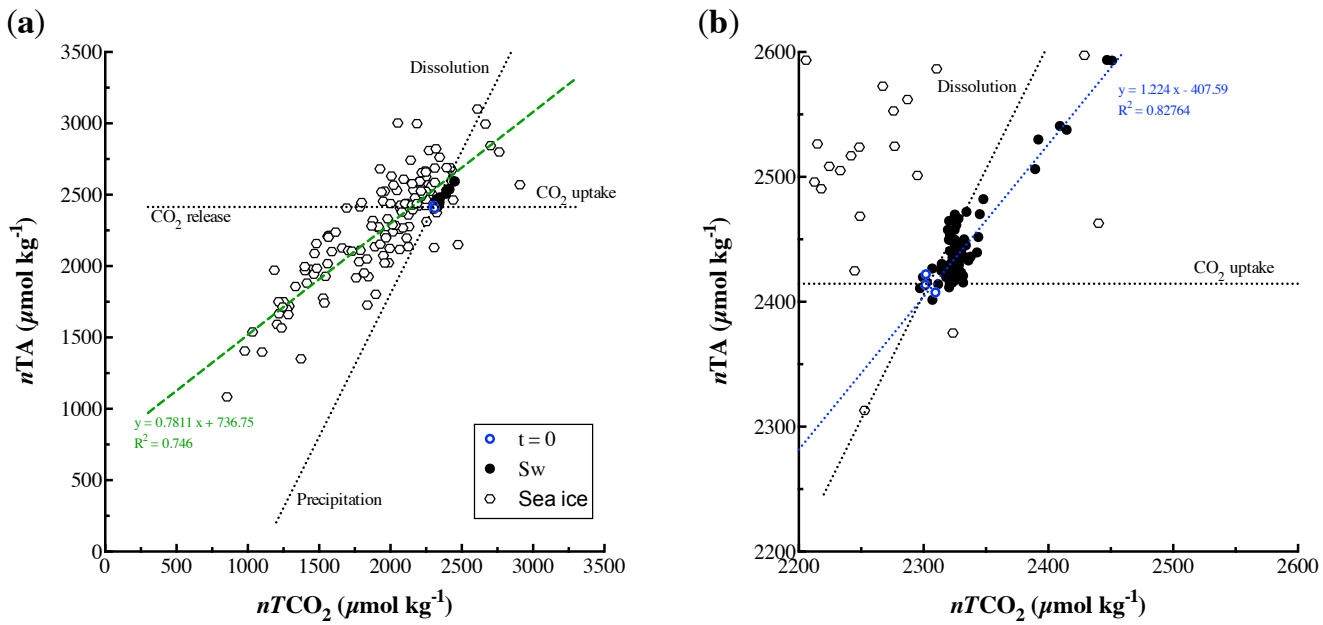

Figure 7: Evolution of (**a**) $TA_{(ice)}$ averaged throughout the ice thickness at each sampling day (black dots) and $TA_{(ice)}^{*}$ (dashed red line) (µmol kg^{-1}) and (**b**) $TCO_{2(ice)}$ averaged throughout the ice thickness at each sampling day (black diamonds) and $TCO_{2(ice)}^{*}$ (dashed red line) (µmol kg^{-1}), (**c**) Estimation of the ikaite precipitation/dissolution from half of the difference between $TA_{(ice)}^{*}$ and $TA_{(ice)}$ (µmol kg^{-1}) (black diamonds) compared to the average amount of ikaite precipitated throughout the ice thickness for each sampling day from Rysgaard et al., (2014) (white dots). The vertical black dotted line on 26 January mark when the heat was turned back ON.

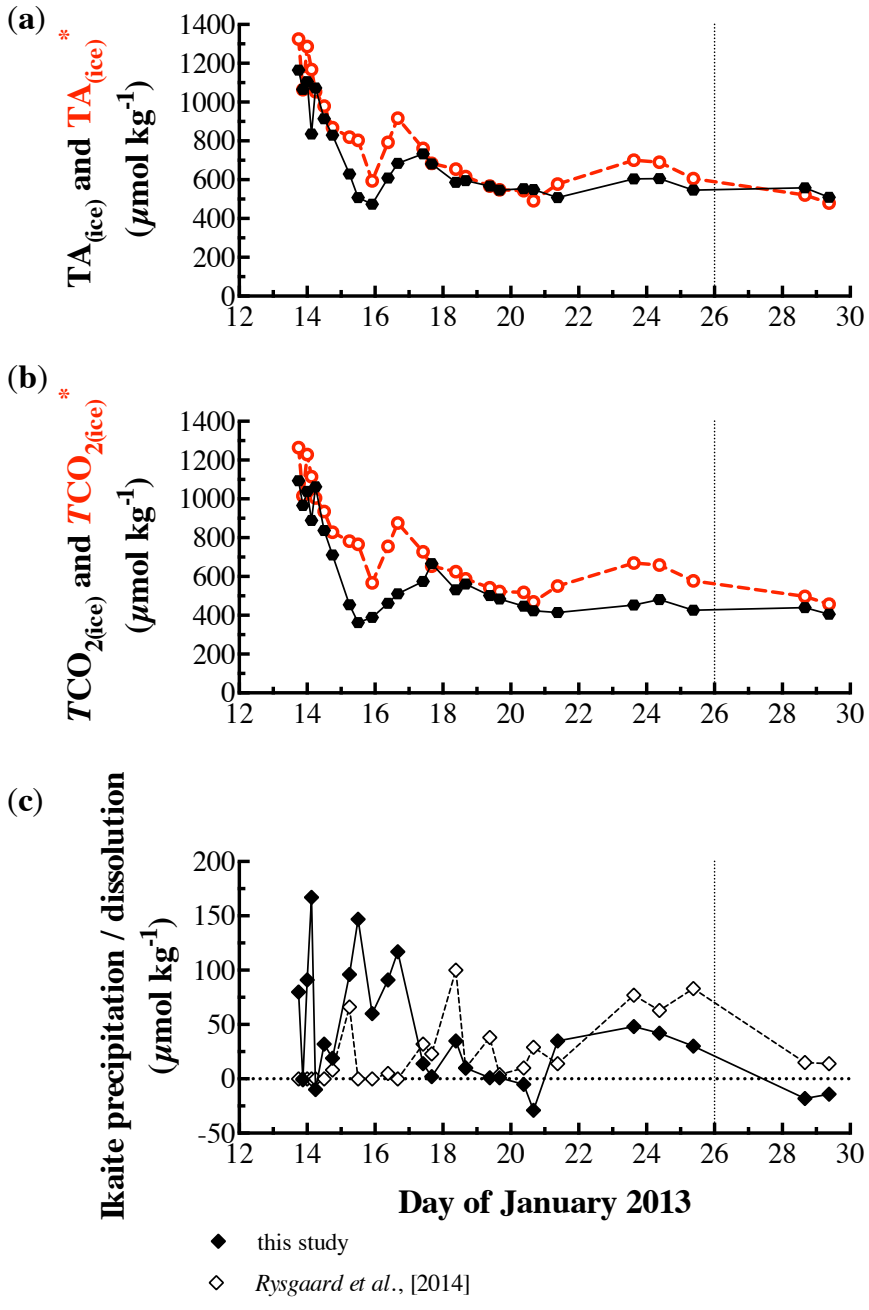

Figure 8: Evolution of (**a**) ikaite dissolution within the water column (in µmol kg^{-1}), (**b**) mass of ikaite dissolved in the underlying seawater (blue), mass of ikaite precipitated in sea ice (black) estimated from this study and estimated from Rysgaard et al., (2014) (white). The vertical black dotted line on 26 January mark when the heat was turned back on.

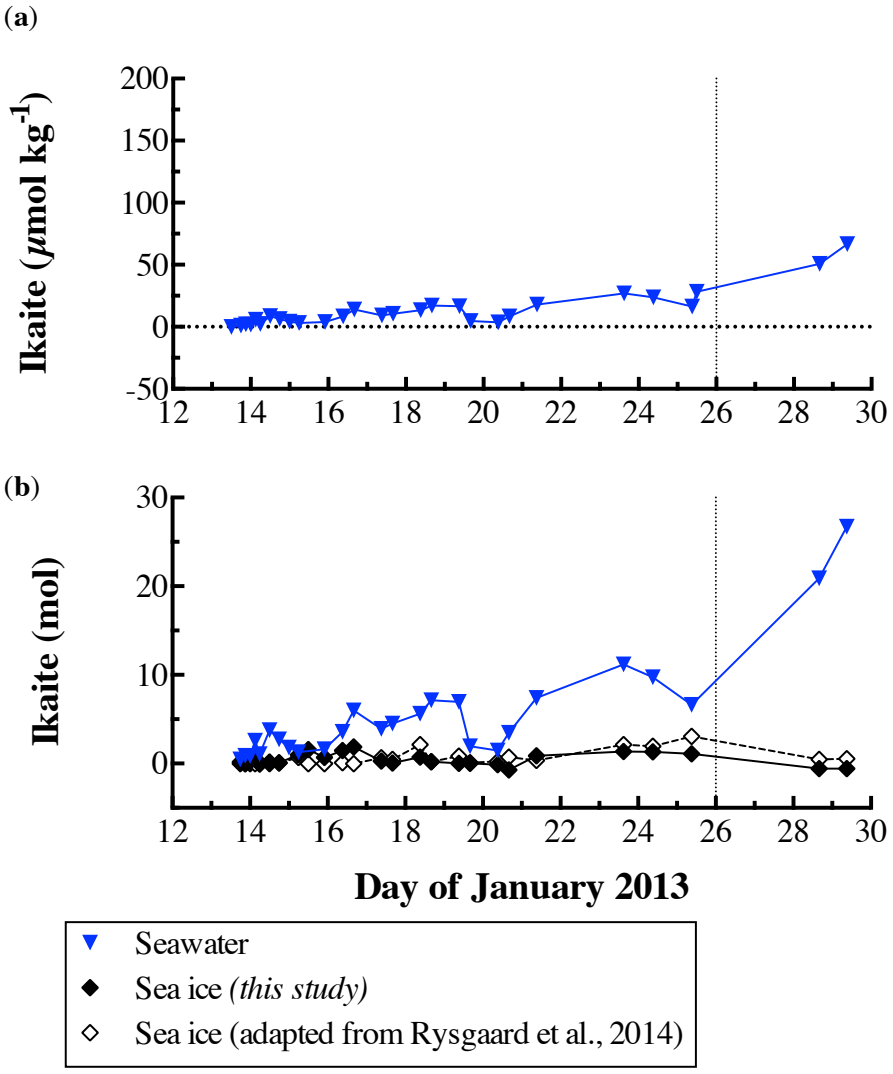

Figure 9: Total amount of TCO_2 lost from the ice cover (black dots), amount of CO_2 exchanges between the atmosphere and the ice cover ($CO_{2air\text{-}ice}$, white triangle) and sea ice-seawater TCO_2 exchanges (blue triangle). In mole for each day, integrated over the whole tank. The dotted line on 26 January mark when the heat was turned back ON.

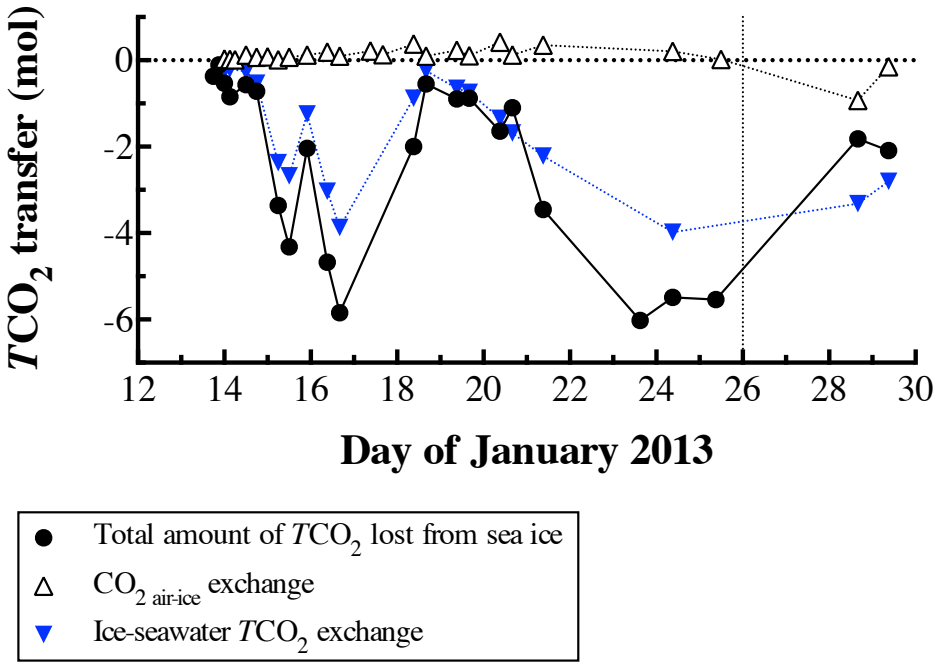

Figure 10: Evolution of (**a**) $\Omega_{aragonite}$ in the water column, calculated based on $TA_{(sw)}$ and $TCO_{2(sw)}$ (black dots) and calculated based on $TA_{(sw)}^{*}$ and $TCO_{2(sw)}^{*}$ (dashed red line) and (**b**) pH in the water column calculated based on $TA_{(sw)}$ and $TCO_{2(sw)}$ (black dots) and calculated based on $TA_{(sw)}^{*}$ and $TCO_{2(sw)}^{*}$ (dashed red line).